

## CellEKT: a robust chemical proteomics workflow to profile cellular target engagement of kinase inhibitors

Rüegger, J.; Gagestein, B.; Janssen, A.P.A.; Valeanu, A.; Mori, A.L.; Peet, M. van der; ...; Lazo Mori, A.A.

#### Citation

Rüegger, J., Gagestein, B., Janssen, A. P. A., Valeanu, A., Mori, A. L., Peet, M. van der, ... Lazo Mori, A. A. (2025). CellEKT: a robust chemical proteomics workflow to profile cellular target engagement of kinase inhibitors. *Molecular And Cellular Proteomics*, 24(6). doi:10.1016/j.mcpro.2025.100961

Version: Publisher's Version

License: Creative Commons CC BY-NC-ND 4.0 license

Downloaded from: <a href="https://hdl.handle.net/1887/4283534">https://hdl.handle.net/1887/4283534</a>

**Note:** To cite this publication please use the final published version (if applicable).

# CellEKT: A Robust Chemical Proteomics Workflow to Profile Cellular Target Engagement of Kinase Inhibitors

#### **Authors**

Joel Rüegger, Berend Gagestein, Antonius P. A. Janssen, Alexandra Valeanu, Alger Lazo Mori, Marielle van der Peet, Michael S. Boutkan, Bogdan I. Florea, Alex A. Henneman, Remo Hochstrasser, Haiyan Wang, Paul Westwood, Andreas Topp, Patricia M. Gomez Barila, Jan Paul Medema, Connie R. Jimenez, Bigna Woersdoerfer, Stephan Kirchner, Jitao David Zhang, Uwe Grether, Arne C. Rufer, and Mario van der Stelt

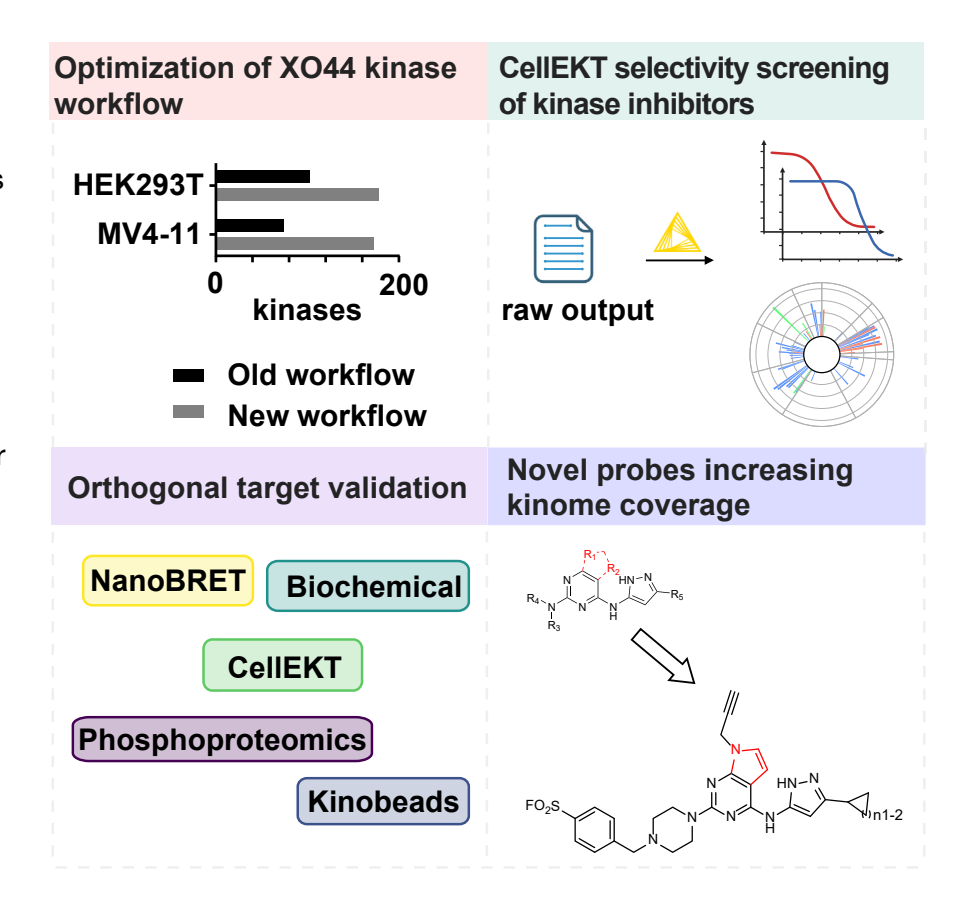
#### Correspondence

m.van.der.stelt@chem. leidenuniv.nl

#### In Brief

In this study, we introduce CellEKT, a chemical proteomics platform designed to assess kinase inhibitor target engagement across a broad range of endogenously expressed kinases. CellEKT expanded the kinome coverage to 48% using novel probes. enabling comprehensive cellular profiling of covalent and noncovalent inhibitor interactions across more than 300 kinases. Validated through phosphoproteomics and NanoBRET, CellEKT offers enhanced insights into kinase selectivity, providing a valuable tool for advancing therapeutic discovery and development.

#### **Graphical Abstract**



#### **Highlights**

- CellEKT is a robust platform for cellular selectivity profiling of kinase inhibitors.
- An experiment-specific peptide library improved detection of low-abundance kinases.
- New broad-spectrum kinase probes, ALX005 and ALX011, expanded kinome coverage beyond XO44 to 48% in total.
- Target validation was performed across different platforms, including phosphoproteomics.
- Automated data analysis workflow validates target engagement of kinase inhibitors.



### **CellEKT: A Robust Chemical Proteomics** Workflow to Profile Cellular Target Engagement of Kinase Inhibitors

Joel Rüegger<sup>1</sup>, Berend Gagestein<sup>1,2</sup>, Antonius P. A. Janssen<sup>1</sup>, Alexandra Valeanu<sup>3</sup>, Alger Lazo Mori<sup>1</sup>, Marielle van der Peet<sup>1</sup>, Michael S. Boutkan<sup>1</sup>, Bogdan I. Florea<sup>4</sup>, Alex A. Henneman<sup>2</sup>, Remo Hochstrasser<sup>3</sup>, Haiyan Wang<sup>3</sup>, Paul Westwood<sup>3</sup>, Andreas Topp<sup>3</sup>, Patricia M. Gomez Barila<sup>5</sup>, Jan Paul Medema<sup>5</sup>, Connie R. Jimenez<sup>2</sup>, Bigna Woersdoerfer<sup>3</sup>, Stephan Kirchner<sup>3</sup>, Jitao David Zhang<sup>3</sup>, Uwe Grether<sup>3</sup>, Arne C. Rufer<sup>3</sup>, and Mario van der Stelt<sup>1,7</sup>

The human genome encodes 518 protein kinases that are pivotal for drug discovery in various therapeutic areas, such as cancer and autoimmune disorders. The majority of kinase inhibitors target the conserved ATP-binding pocket, making it difficult to develop selective inhibitors. To characterize and prioritize kinase-inhibiting drug candidates, efficient methods are desired to determine target engagement (TE) across the cellular kinome. In this study, we present CellEKT (Cellular Endogenous Kinase Targeting), an optimized and robust chemical proteomics platform for investigating cellular TE of endogenously expressed kinases using the sulfonyl fluoride-based probe XO44 and two new probes ALX005 and ALX011. The optimized workflow enabled the determination of the kinome interaction landscape of covalent and noncovalent drugs across over 300 kinases, expressed as IC<sub>50</sub>, which were validated using distinct platforms like phosphoproteomics and NanoBRET. With CellEKT, TE profiles were linked to their substrate space. CellEKT has the ability to decrypt drug actions and to guide the discovery and development of drugs.

Kinases are important enzymes that phosphorylate proteins or cellular metabolites, regulating protein function, signaling pathways, and cellular function. The human genome encodes 637 kinases with 518 targeting proteins and others phosphorylating lipids, carbohydrates, or other metabolites (1, 2). Kinase dysregulation is linked to diseases like cancer, inflammatory conditions, and autoimmune disorders, making kinases vital drug targets (3). The discovery of kinase inhibitors is a major

focus in both academic and industrial research, culminating in the 80 Food and Drug Administration (FDA)-approved kinase inhibitors as of writing (4). Many inhibitors target the conserved ATP-binding site in kinases, often leading to off-target interactions resulting in adverse side effects (5). Due to toxicity and efficacy issues, most kinase inhibitors fail in clinical trials, with only 41% successfully progressing from phase I to regulatory approval (6). Thus, understanding the interactions of kinase inhibitors with their targets is crucial, especially as they are developed for nononcological conditions (3).

To study the selectivity profile of kinase inhibitors binding and activity assays with purified kinases or their catalytic domains, along with mass spectrometry (MS)-based methods, are commonly used. These include irreversible ATP/ ADP-biotin probes (7, 8) (KiNativ platform), photoaffinitybased probes (9), and Kinobeads (10-12). However, these assays fail to replicate the complex cellular environment, which can influence enzyme activity through post-translational modifications, cellular localization, substrate levels, and protein-protein interactions (13, 14). Kinase inhibitors targeting the ATP-binding site must also compete with cellular ATP, present at 2 to 8 mM in mammalian cells, which is two to three orders of magnitude higher than the enzyme  $K_M$ , frequently used in biochemical assays under balanced conditions (15, 16). This discrepancy can lead to different cellular target engagement (TE) profiles compared with those obtained from biochemical and lysate-based assays.

To address these limitations, several methods have been developed to study TE in living cells. The cellular thermal shift

From the <sup>1</sup>Department of Molecular Physiology, Leiden Institute of Chemistry, Leiden University & Oncode Institute, Leiden, The Netherlands; <sup>2</sup>Department Medical Oncology, OncoProteomics Laboratory, Cancer Center Amsterdam, Amsterdam UMC, Amsterdam, The Netherlands; <sup>3</sup>Roche Pharma Research & Early Development, Roche Innovation Center Basel, F. Hoffmann-La Roche Ltd, Basel, Switzerland; <sup>4</sup>Bio-Organic Synthesis, Leiden Institute of Chemistry, Leiden University, Leiden, The Netherlands; <sup>5</sup>Laboratory for Experimental Oncology and Radiobiology, Center for Experimental and Molecular Medicine, Cancer Center Amsterdam, Amsterdam UMC, University of Amsterdam and Oncode Institute, Amsterdam, The Netherlands

<sup>\*</sup>For correspondence: Mario van der Stelt, m.van.der.stelt@chem.leidenuniv.nl.



assay (CETSA) (17) is a powerful technology for full proteome drug target screenings (18) and has been successfully applied to in vivo studies and whole blood samples (19). However, low-abundant, membrane-bound, or unstable targets are challenging to assess with CETSA, which may result in overlooked drug interactions (17).

Another technology for cellular selectivity screening is the Nanoluciferase (NanoLuc; Nluc)-based bioluminescence resonance energy transfer (NanoBRET) assay, which has been applied across different enzyme classes (20, 21). NanoBRET has advanced the selectivity screening of kinase inhibitors, assessing inhibitor specificity across a spectrum of 178 kinases in a 96-well format in transfected human embryonic kidney 293 (HEK293) cells (16). Refinements in the NanoBRET platform have allowed the substitution of six BRET tracers with a single one and extended the coverage to 192 kinases (22) with the capability to perform automated screenings in a 384-well format (23). Despite these advancements, this platform relies on overexpressed and transfected constructs, limiting its applicability across different biological systems, such as various cell lines, organoids, animal models, or primary human cells (24, 25).

Chemical proteomics has emerged as a powerful technique to assess the target interaction landscape of small molecules using chemical probes in a native biological context. XO44 was the first kinase probe developed for this purpose (26). It is a broad-spectrum kinase inhibitor with a sulfonyl fluoride warhead that reacts covalently with a conserved lysine in the kinase pocket. It also includes a bio-orthogonal ligation handle for attaching a fluorophore for visualization or a biotin for affinity enrichment. In the original work, XO44 was used to identify 133 kinases in Jurkat cells and to map the cellular target-interaction landscape of dasatinib. In addition, XO44 was used to study kinome expression in lenvatinib-resistant hepatocellular carcinoma cells, identifying cyclin-dependent kinase 6 (CDK6) as a resistance driver (27). Modifications to the scaffold of XO44 have included a salicylaldehyde warhead to determine the target profile of a CDK inhibitor in mice (28) and substituted aryl fluorosulfates to profile the kinase lysine reactivity (29). These studies show the value of chemical proteomics in establishing TE studies in native biological settings. Although XO44 is commercially available, thereby facilitating broad usage of this probe, no best practices for its use have been reported.

Here, we report a refined chemical proteomics workflow, named CellEKT (Cellular Endogenous Kinase Targeting), which builds on our previously reported chemical proteomics workflow (30, 31) and is inspired by the work of Taunton et al. (26, 28). This approach profiles the cellular TE of kinase inhibitors using XO44 and two new chemical probes. By employing CellEKT, we profiled the cellular interaction landscape of the FDA-approved kinase inhibitors dasatinib, midostaurin, and three Bruton's tyrosine kinase (BTK) inhibitors. The targets of these drugs identified by CellEKT were validated through diverse methodologies, including biochemical assays, NanoBRET technology, and phosphoproteomic analysis. Finally, by leveraging resources of protein kinase substrate specificity (32, 33) and computational tools (34), we show that CellEKT helps to define substrate space and elucidate drug mechanisms and off-target effects. In summary, CellEKT serves as a refined tool to gain a comprehensive understanding of therapeutic and toxicological mechanisms of actions for kinase drug discovery.

#### EXPERIMENTAL PROCEDURES

The antibodies, buffers, and reagents used in this study are listed in Table 1.

#### Cell Culture

Colo320-HSR (female human origin) and MDST8 (gender undetermined) cells were cultured at 37 °C under 7% CO2 in RPMI1640 (R5886; Merck) with GlutaMAX, 1% glucose (G8769; Merck), 10% fetal calf serum (FCS) (Thermo Fisher), 1 mM sodium pyruvate, and penicillin and streptomycin (200 µg/ml each; Duchefa). Cells were passaged twice a week at 80 to 90% confluence by trypsinization.

HeLa (female human origin) and U2OS (female human origin) cells were cultured at 37 °C under 7% CO<sub>2</sub> in Dulbecco's modified Eagle's medium (DMEM) (D6546; Merck) with GlutaMAX, 10% newborn calf serum (Thermo Fisher), and penicillin and streptomycin (200 μg/ml each). Cells were passaged twice a week at 80 to 90% confluence by trypsinization.

SK-N-SH (female human origin) and U-87 (male human origin) cells were cultured at 37 °C under 7% CO2 in DMEM (D6546) with Gluta-MAX, 10% FCS, and penicillin and streptomycin (200 μg/ml each). Cells were passaged twice a week at 80 to 90% confluence by trypsinization.

Hs 578T (female human origin) and MDA-MB-231 (female human origin) cells were cultured at 37 °C under 7% CO2 in RPMI1640 (R5886) with GlutaMAX, 10% FCS, and penicillin and streptomycin (200 μg/ml each). Cells were passaged twice a week at 80 to 90% confluence by trypsinization.

RPE-1 (female human origin) cells were cultured at 37 °C under 7% CO<sub>2</sub> in in DMEM/F12 (D8062; Merck) with GlutaMAX, 10% FCS, and penicillin and streptomycin (50 µg/ml each). Cells were passaged twice a week at 80 to 90% confluence by trypsinization.

HT-29 (female human origin) cells were cultured at 37 °C under 7% CO<sub>2</sub> in DMEM (D6546) with GlutaMAX, 5% FCS, 10 mM Hepes, and penicillin and streptomycin (200 µg/ml each). Cells were passaged twice a week at 80 to 90% confluence by trypsinization.

HuTu-80 (male human origin) cells were cultured at 37 °C under 7% CO<sub>2</sub> in DMEM/F12 (D8062) with GlutaMAX, 10% FCS, 10 mM Hepes, and penicillin and streptomycin (200 μg/ml each). Cells were passaged twice a week at 80 to 90% confluence by trypsinization.

HEK293T (female human origin) cells were cultured at 37 °C under 7% CO<sub>2</sub> in DMEM (D6546) with GlutaMAX, 10% newborn calf serum, and penicillin and streptomycin (200 µg/ml each). Cells were passaged twice a week at 80 to 90% confluence by resuspension in fresh medium.

A375 (female human origin), AMO1 (female human origin), K562 (female human origin), and THP-1 (male human origin) cells were cultured at 37 °C under 7% CO<sub>2</sub> in RPMI1640 (R5886) with GlutaMAX, 10% FCS, 1 mM sodium pyruvate, and penicillin and streptomycin (200 μg/ml each).



TABLE 1 Antibodies, buffers, and reagents

Reagent	Source	Identifier
Antibodies		
Anti-FES (1:1000 dilution)	Cell Signaling Technologies	Catalog no.: 85704
Anti-rabbit-HRP (1:4000 dilution)	Santa Cruz Biotechnologies	Catalog no.: sc-2030
Chemicals, peptides, and recombinant proteins	· ·	· ·
Benzonase	Santa Cruz Biotechnology	Catalog no.: sc-202391
Biotin-azide	Santa Cruz Biotechnology	Catalog no.: sc-485768
Lipid-free BSA	Merck	Catalog no.: A7030
Empore Extraction Disks	Phenomenex	Catalog no.: AH0-2540
DPBS	Merck	Catalog no.: D8537
Pierce High Capacity Streptavidin Agarose	Thermo Fisher	Catalog no.: 20361
Micro tube 1.5 ml LB	Sarstedt	Catalog no.: 72.706.600
cOmplete EDTA-free Protease Inhibitor Cocktail	Merck	Catalog no.: 11873580001
Pierce Avidin Agarose	Thermo Fisher	Catalog nos.: 20219, 20225
Pierce Control Agarose	Thermo Fisher	Catalog no.: 26150
High-recovery sample vials	Screening Devices	Catalog no.: KG 09 1122
Triton X-100	Merck	Catalog no.: T8787
Trypsin, sequencing grade	Promega	Catalog no.: V5111
XO44 (PF-6808472)	Merck	Catalog no.: PZ0306
Yeast enolase digest	Waters	Catalog no.: 186002325
CuSO <sub>4</sub>	Merck	Catalog no.: 61230
TCEP.HCI	Merck	Catalog no.: C4706
THPTA	Merck	Catalog no.: 762342
TAMRA-bioin-azide	Click Chemistry Tools	Catalog no.: 1048
RPMI1640	Merck	Catalog no.: R5886
DMEM high glucose	Merck	Catalog no.: D6546
DMEM/F12	Merck	Catalog no.: D8062
IMDM	Merck	Catalog no.: I3390
Penicillin G Sodium	Duchefa	Catalog no.: P0142
Streptomycin sulphate	Duchefa	Catalog no.: S0148
FCS	VWR	Catalog no.: 97068-085
Newborn calf serum	VWR	Catalog no.: 10158-358
Horse serum, heat inactivated	Thermo Fisher	Catalog no.: 26050070
GlutaMAX	Thermo Fisher	Catalog no.: 35050061
Phorbol-12-myristate-13-acetate	Focus Biomolecules	Catalog no.: 10-2165
Staurosporin	MedChemExpress	Catalog no.: HY-15141
AlexaFluor 647-azide (AF647-N3)	Thermo Fisher	Catalog no.: A10277
Midostaurin	MedChemExpress	Catalog no.: HY-10230
Ibrutinib	MedChemExpress	Catalog no.: HY-10997
Acalabrutinib	MedChemExpress	Catalog no.: HY-17600
Zanubrutinib	MedChemExpress	Catalog no.: HY-101474A
Dasatinib	MedChemExpress	Catalog no.: HY-10181
FP-alkyne	Janssen et al. (30)	Not available
Biotin	Thermo Scientific	Catalog no.: 29129
Critical commercial assays		
Pierce BCA Protein Assay Kit	Thermo Fisher	Catalog no.: 23225
KINOMEscan Profiling Service	DiscoverX	www.discoverx.com

TK6 (male human origin) cells were cultured at 37 °C under 7% CO<sub>2</sub> in RPMI1640 (R5886) with GlutaMAX, 10% horse serum (Thermo Fisher), 1 mM sodium pyruvate, and penicillin and streptomycin (200 μg/ml each).

MV4-11 (male human origin) and SEM (female human origin) cells were cultured at 37 °C under 5% CO<sub>2</sub> in Iscove's modified Dulbecco's medium (IMDM) (I3390; Merck) with GlutaMAX, 10% FCS, and penicillin and streptomycin (200 µg/ml each).

THP-1 cells were differentiated and stimulated by plating 3.0  $\times$ 10<sup>6</sup> cells in 6 cm dishes in 5 ml complete RPMI1640 containing 20 ng/ml phorbol-12-myristate-3-acetate (Focus Biomolecules) for 24 h. Then, medium was replaced with serum-free RPMI1640 with 0.1% delipidated bovine serum albumin (BSA) (Merck) with GlutaMAX, 1 mM sodium pyruvate, and penicillin and streptomycin (M0-like) for 24 h. Cell lines were tested regularly for mycoplasma contamination, and all tests were negative. Cultures were discarded after 2 to 3 months of use.

#### Cell Treatment for Chemical Proteomics

Adherent cells were cultured in 6-well plates or 6 cm dishes (Sarstedt) and grown to 80 to 90% confluency, aiming to recover approximately 0.75 mg of total protein per condition after lysis. Prior to treatment, the growth medium was aspirated, and the cells were gently washed with 2 ml Dulbecco's PBS (DPBS). Cells were treated with kinase inhibitor (1.11X) or vehicle (0.111% dimethyl sulfoxide [DMSO]) in the corresponding serum-free culture medium supplemented with 0.1% delipidated BSA and in case of IMDM or DMEM with additional 10 mM Hepes (treatment medium). The kinase inhibitor was tested at six concentrations ranging from 0.1 to 10,000 nM in n = 2 biological replicates per concentration (12 samples total). Vehicle treatments were conducted across 10 samples, including negative control (n = 2), positive control (n = 4), and peptide library treatments (n = 4). Cells were incubated with the kinase inhibitor or vehicle at 37 °C for 1 h. Following this, a solution of XO44 (10X for positive control and competition samples or 100X for peptide library samples) or vehicle (1% DMSO or 0.2% DMSO final) was added in treatment medium. Cells were incubated at 37 °C for an additional 30 min. The medium was aspirated, and treatment was halted by the addition of 1 ml ice-cold DPBS. Cells were then scraped off on ice, collected into 1.5 ml Eppendorf tubes, and spun down again (1000g, 5 min, 4 °C). The supernatant was removed, and cell pellets were snap-frozen in liquid nitrogen and stored at -80 °C.

For cell line screening or probe profiling experiments, the initial 1 h incubation step was omitted, and cells were incubated with the probe (n = 3) or vehicle (n = 2) for 30 min directly before proceeding with

Suspension cells in log phase were spun down (300g, 5 min) and resuspended at 1.0 × 10<sup>6</sup> cells per ml in the corresponding serumfree culture medium supplemented with 0.1% delipidated BSA and in case of IMDM or DMEM, 10 mM Hepes. Amount of total cells was adjusted to receive approximately 0.75 mg of final protein after cell lysis. Cells were treated with kinase inhibitor (1.11X) or vehicle (0.111% DMSO). The kinase inhibitor was tested at six concentrations ranging from 0.1 to 10,000 nM in n = 2 biological replicates per concentration (12 samples total). Vehicle treatments were conducted across 10 samples, including negative control (n = 2), positive control (n = 4), and peptide library treatments (n = 4). Cells were incubated with the kinase inhibitor or vehicle at 37 °C for 1 h. Following this, a solution of XO44 (10X for positive control and competition samples or 100X for peptide library samples) or vehicle (1% DMSO or 0.2% DMSO final) was added in treatment medium. Cells were incubated for an additional 25 min at 37 °C. Cells were spun down (300g, 5 min, 37 °C), resuspended in ice-cold DBPS (1 ml), collected into 1.5 ml Eppendorf tubes, and spun down again (1000g, 5 min, 4 °C). The supernatant was removed, and cell pellets were snap-frozen in liquid nitrogen and stored at -80 °C.

For cell line screening or probe profiling experiments, the initial 1 h incubation step was omitted, and cells were incubated with the probe (n = 3) or vehicle for 30 min directly before proceeding with collection.

#### Chemical Proteomics Assay for Cell Line Screen

Screening the cell lines was performed with a method adapted from previous experience with chemical proteomics (30) and usage of XO44 as a kinase probe (26) with modifications based on the gel-based results. Cell pellets were lysed completely by vortexing in 400 µl icecold lysis buffer containing 50 mM Hepes (pH 7.5), 150 mM NaCl, 1 mM MgCl<sub>2</sub>, 0.1% (w/v) Triton X-100, 1X cOmplete EDTA-free Protease Inhibitor Cocktail (Roche), and 25 U/ml benzonase (sc-202391; Santa Cruz). Protein concentrations were measured by bicinchoninic acid (BCA) assay (Thermo Fisher), equalized, and 360 µl lysate was transferred to 2 ml Eppendorf tubes containing 40 µl 10% SDS (1% final), vortexed, and left at room temperature (RT).

The lysates were subjected to a click reaction for 1 h with freshly prepared click mix (31.2 μl per sample: 16 μl 25 mM CuSO<sub>4</sub> in MilliQ, 3.2 µl 25 mM Tris(3-hydroxypropyltriazolylmethyl)amine [THPTA] in DMSO, 4  $\mu$ l 2.5 mM biotin-N<sub>3</sub> in DMSO, and 8  $\mu$ l 50 mM Tris(2carboxyethyl)phosphine hydrochloride [TCEP.HCI] freshly dissolved in DPBS). Proteins were precipitated by addition of Hepes buffer (80 μl, 50 mM Hepes; pH 7.5), methanol (MeOH) (666 μl), CHCl<sub>3</sub> (166 µl), and MilliQ (150 µl), vortexing after each addition. After spinning down (1500g, 10 min), the upper and lower layers were aspirated and the protein pellet was resuspended in MeOH (600 µl) by sonication (Qsonica Q700 Microplate Sonicator, 2 × 10 s pulses, 10% amplitude). The protein was spun down (20,000g, 5 min), and the supernatant was discarded. The proteins were redissolved in 6 M urea (500 µl) with 25 mM NH<sub>4</sub>HCO<sub>3</sub> for 15 min, followed by reduction (65 °C, 15 min, 800 rpm shaking) with DTT (5 µl, 1 M in MilliQ). The samples were allowed to reach RT, and proteins were alkylated (30 min) with iodoacetamide (IAA) (40 μl, 0.5 M in MilliQ) in the dark. SDS (140 μl; 10% w/v) was added, and the samples were spun down (1000g, 5 min). The samples were then transferred to 15 ml Falcon tubes containing 5 ml PBS and 100  $\mu$ l avidin agarose slurry (Pierce; 100  $\mu$ l of a 50% slurry, prewashed twice with 6 ml PBS + 0.5% SDS and once with 6 ml PBS), and the samples were incubated for 2 h while rotating. The beads were then spun down (2000g, 2 min) and washed (3  $\times$ PBS + 0.5% SDS, 2x PBS, and 1x MilliQ). The beads were resuspended in digestion buffer (250 µl, 100 mM Tris [pH 7.8], 100 mM NaCl, 1 mM CaCl<sub>2</sub>, 2% [v/v] acetonitrile [ACN], sequencing grade trypsin [Promega; 0.25 µg]), transferred to low-binding tubes (Sarstedt), and incubated while shaking in Eppendorf tube shaker overnight (16 h, 37 °C, 1000 rpm). Trypsin was quenched with 12.5 µl formic acid (FA; ULC-MS grade), and the beads were removed by filtration using a Bio-Spin column (Bio-Rad, 400g, 5 min), collecting the flow-through in a new 2 ml tube. Peptides were desalted using C18 StageTips (35) preconditioned with 50 µl MeOH, 50 µl of 0.5% (v/v) FA in 80% (v/v) ACN/MilliQ (solution B), and 50 μl 0.5% (v/v) FA in MilliQ (solution A) by centrifugation (600g, 1-2 min). The peptides on the StageTip were washed with solution A (100 µl) and eluted into new low-binding tubes using solution B (100 µl). Samples were concentrated using an Eppendorf speedvac (Eppendorf Concentrator Plus 5301).

#### CellEKT Workflow

The optimized chemical proteomics workflow incorporates the improvements made based on the chemical proteomics optimization experiments. Cells were treated with kinase inhibitor and probe as described in the section "Cell treatment for chemical proteomics" and snap-frozen. HEK293T cells (1.5  $\times$  10<sup>6</sup>) and MV4-11 cells (7  $\times$  10<sup>6</sup>) were used to receive approximately 0.75 mg of final protein after cell lysis for each condition. Kinase inhibitors are tested in a full doseresponse manner at six different concentrations from 0.1 to 10,000 nM with each concentration in biological duplicates (n = 2). In addition, n = 4 biological replicates as positive control and peptide library samples are included by treating cells with 1 or 10  $\mu M$  probe, respectively. All resulting cell pellets were lysed by vortexing in 400 μl ice-cold lysis buffer containing 50 mM Hepes (pH 7.5), 150 mM NaCl, 1 mM MgCl<sub>2</sub>, 0.1% (w/v) Triton X-100, 1X cOmplete EDTA-free Protease Inhibitor Cocktail, and 25 U/ml benzonase (sc-202391). Protein concentrations were measured by BCA assay, equalized, and 360 µl lysate was transferred to 2 ml Eppendorf tubes containing 40 µl 10% SDS (1% final), vortexed, and left at RT.

The lysates were subjected to a click reaction for 1 h with freshly prepared click mix (31.2 μl per sample: 16 μl 25 mM CuSO<sub>4</sub> in MilliQ, 3.2  $\mu$ l 25 mM THPTA in DMSO, 4  $\mu$ l 10 mM biotin-N<sub>3</sub> in DMSO, and 8  $\mu$ l 50 mM TCEP.HCl freshly dissolved in DPBS). Proteins were precipitated by addition of Hepes-EDTA buffer (80 µl, 50 mM Hepes, 50 mM EDTA, pH 7.5), MeOH (666  $\mu$ l), CHCl<sub>3</sub> (166  $\mu$ l), and MilliQ (150  $\mu$ l), vortexing after each addition. After spinning down (1500g, 5 min), the upper and lower layers were aspirated, and the protein pellet was resuspended in MeOH (600 µl) by sonication (Qsonica Q700 Microplate Sonicator, 2 × 10 s pulses, 10% amplitude).

The protein was spun down (20,000g, 5 min), and the supernatant was discarded. The proteins were redissolved in 0.5% SDS in PBS (500 µl) containing 5 mM DTT by heating (65 °C, 15 min, 800 rpm shaking). Samples were allowed to reach RT and treated with IAA (15 µl, 0.5 M in MilliQ, 10 mM final) for 30 min at RT. Samples were spun down briefly (20,000g, 2 min), inspected for undissolved material, and the supernatant was transferred to new 1.5 ml Eppendorf tubes containing prewashed beads.

Beads were prepared by mixing 10  $\mu$ l high-capacity streptavidin agarose (Pierce, 20 µl of a 50% slurry) with 10 µl control agarose (Pierce, 20 µl of a 50% slurry) and washing the mixture twice with PBS + 0.5% SDS and once with PBS by vortexing, spinning down (3000g, 2 min), and discarding the supernatant at each step. The beads were suspended in 500  $\mu l$  PBS containing 10 mM DTT before addition of the protein sample.

After the sample and beads were combined, the mixture was agitated by shaking (1000 rpm, 2 h). The beads were then spun down (3000g, 2 min), supernatant was discarded, and the beads were washed (3 × PBS + 0.5% SDS, 3x PBS) by vortexing, spinning down (3000g, 2 min), and discarding the supernatant at each step. The beads were resuspended in MilliQ, transferred to low-binding tubes, spun down (3000g, 2 min), and the supernatant was aspirated. Then, beads were suspended in digestion buffer (200 µl, 100 mM Tris [pH 7.8], 100 mM NaCl, 1 mM CaCl<sub>2</sub>, 2% [v/v] ACN, sequencing grade trypsin [0.5 μg]) and incubated while shaking overnight (16 h, 37 °C, 1000 rpm). Trypsin was guenched by addition of a solution of 10% (v/v) aqueous (aq.) FA, the beads were spun down (3000g, 2 min), and the peptides in the supernatant were desalted using C18 StageTips (35) preconditioned with 50 µl MeOH, 50 µl of 0.5% (v/v) FA in 80% (v/v) ACN/MilliQ (solution B), and 50  $\mu$ l 0.5% (v/v) FA in MilliQ (solution A) by centrifugation (600g, 1-2 min). The peptides on the StageTips were washed with solution A (100 µl) and eluted into new low-binding tubes using solution B (100 μl). Samples were concentrated using an Eppendorf speedvac (Eppendorf Concentrator Plus 5301).

#### Nano-LC-MS Settings for Pulldown Samples

Desalted peptide samples were reconstituted in 30 µl LC-MS solution (97:3:0.1 H<sub>2</sub>O:ACN:FA) containing 10 fmol/μl yeast enolase digest (catalog no.: 86002325; Waters) as injection control. Injection amount was titrated using a pooled quality control sample to prevent overloading the nanoLC system and the automatic gain control (AGC) of the QExactive HF mass spectrometer.

The desalted peptides were separated on a UltiMate 3000 RSLCnano system set in a trap-elute configuration with a nanoEase M/Z Symmetry C18 100 Å, 5  $\mu$ m, 180  $\mu$ m  $\times$  20 mm (Waters) trap column for peptide loading/retention and nanoEase M/Z HSS C18 T3 100 Å, 1.8  $\mu$ m, 75  $\mu$ m  $\times$  250 mm (Waters) analytical column for peptide separation. The column was kept at 40 °C in a column oven.

Samples were injected on the trap column at a flow rate of 15 µl/min for 2 min with 99% mobile phase A (0.1% FA in ULC-MS grade water [Biosolve]) and 1% mobile phase B (0.1% FA in ULC-MS grade ACN [Biosolve]) eluent. The 85 min LC method, using mobile phase A and mobile phase B controlled by a flow sensor at 0.3 µl/min with average pressure of 400 to 500 bar (5500-7000 psi), was programmed as gradient with linear increment to 1% B from 0 to 2 min, 5% B at 5 min, 22% B at 55 min, 40% B at 64 min, 90% B at 65 to 74 min, and 1% B at 75 to 85 min. The eluent was introduced by electrospray ionization (ESI) via the nanoESI source (Thermo) using stainless steel Nano-bore emitters (40 mm, outer dimater 1/32", ES542; Thermo Scientific).

The QExactive HF was operated in positive mode with datadependent acquisition (DDA) without the use of lock mass, default charge of 2+, and external calibration with LTQ Velos ESI positive ion calibration solution (catalog no.: 88323; Pierce, Thermo) every 5 days to less than 2 ppm. The tune file for the survey scan was set to scan range of 350 to 1400 m/z, 120,000 resolution (m/z 200), one microscan, AGC of 3e6, maximum injection time of 100 ms, no sheath, aux or sweep gas, spray voltage ranging from 1.7 to 3.0 kV, capillary temperature of 250 °C, and an S-lens value of 80. For the 10 datadependent MS/MS events, the loop count was set to 10 and the general settings were resolution to 15,000, AGC target 1e5, maximum injection time 50 ms, isolation window of 1.6 m/z, fixed first mass of 120 m/z, and normalized collision energy of 28 eV. For individual peaks, the data-dependent settings were 1.00e3 for the minimum AGC target yielding an intensity threshold of 2.0e4 that needs to be reached prior of triggering an MS/MS event. No apex trigger was used, unassigned, +1, and charges >+8 were excluded with peptide match mode preferred, isotope exclusion on, and dynamic exclusion of 10 s.

In between experiments, routine wash and control runs were done by injecting 5 μl LC-MS solution containing 5 μl of 10 fmol/μl BSA or enolase digest and 1 µl of 10 fmol/µl angiotensin III (Fluka, Thermo)/ oxytocin (Merck) to check the performance of the platform on each component (nano-LC, the mass spectrometer [mass calibration/ quality of ion selection and fragmentation] and the search engine).

#### MaxQuant Processing

Raw files were analyzed with MaxQuant (version 1.6.17.0 for the cell line screen, version 2.0.1.0 for all other experiments; Cox lab, Max Planck Institute of Biochemistry). The following changes were made to the standard settings of MaxQuant: label-free quantification (LFQ) was enabled with an LFQ minimal ratio count of 1. Match between runs (MBR) and intensity-based absolute quantification were enabled. Searches were performed against a UniProt database of the human proteome (UPID: UP000005640, 20,361 entries downloaded on August 14, 2020) including yeast enolase (P00924). Enzyme specificity was set to Trypsin/P, and up to two missed cleavages were allowed. Cysteine carboxamidomethylation (+57.021464 Da) was treated as fixed modification and methionine oxidation (+15.994915 Da) and Nterminal acetylation (+42.010565 Da) as variable modifications. The mass tolerance for precursor was set to 20 ppm in the first search and 4.5 ppm in the main search. The fragment mass tolerance was set to 20 ppm. False discovery rate (FDR) at peptide and protein levels was set to 1%. The "peptides.txt" and "proteingroups.txt" files were used for further analysis in Microsoft Excel, GraphPad Prism 8.1.1 (Graph-Pad Software, Inc), and KNIME Analytics Platform 4.5.2. "Probeenriched kinases" were defined by filtering the UniProt ID for human reviewed proteins annotated with keyword "Kinase" (KW-0418) in UniProt (Supplemental Table S1), a fold change in LFQ of at least two between positive (XO44 treatment) and negative control (vehicle treatment), two or more unique peptides detected, and at most one missing LFQ value in the positive control replicates. For KNIME processing, enrichment was based on protein intensity instead of LFQ intensity as this afforded more relevant results.

#### Data Analysis in KNIME

The data analysis workflow was built in KNIME Analytics Platform 4.5.2 with two additional modules: KNIME Python Integration and the Vernalis KNIME nodes. The workflow is fully annotated to provide insight in the data analysis steps. A sample list template has been created in Microsoft Excel that provides a convenient user input for the automated workflow. The sample list template is used to crosscorrelate .raw file names and treatment conditions as well as define proteins of interest (POIs). This sample list, together with the Max-Quant output, is read in by KNIME. Here, in brief, the MaxQuant output is sanitized by removal of reverse peptides and contaminants, and

grouped identifications are split toward their first (predominant) identification. Proteins with fewer than two unique peptides (configurable) are removed. A Gaussian distribution is fitted through all log<sub>2</sub>-transformed LFQ values using Pythons SciPy norm.fit. This distribution is then transformed by shifting  $\mu$  left 1.8 $\sigma$  and reducing  $\sigma$  by 70% as per default settings of Perseus developed by Tyanova et al. (36). This resulting normal distribution is used to impute missing values for enriched proteins. Enrichment of proteins in probe-treated positive controls versus DMSO-treated negative controls is calculated based on raw intensity values, and all proteins with a ratio ≥2 are considered probe targets. Further quality filtering is performed by ensuring that the positive controls have at most one missing LFQ intensity value. For the resulting enriched proteins, missing values are imputed, and LFQ intensities are normalized with respect to mean unimputed positive control values. Proteins where the highest concentration of inhibitor shows ≤60% probe labeling are flagged for pIC<sub>50</sub> fitting. The IC50 and Hill slope are fitted using Pythons SciPy optimize.curve\_fit algorithm using the equation:

$$\%Effect = \frac{100}{1 + e^{Hill^*(\log([inhibitor]) - \log(EC_{50}))}}$$

where Hill is the Hill slope and [inhibitor] is the concentration of inhibitor used. This procedure and its output fits with error estimates is identical to standard IC<sub>50</sub> curve fitting algorithms such as integrated in applications such as GraphPad Prism and relevant R-packages. Initial values for Hill slope and IC<sub>50</sub> are provided as 1 and 1000 nM, respectively. The Hill slope is constrained to be fit between 0 and 5. Determined pIC<sub>50 values</sub> are classified as "Good" if  $0.3 \le Hill$  slope  $\le 3.0$ ,  $\sigma(pIC_{50}) \le 0.5$ , and  $pIC_{50} \ge Max(p[inhibitor])$ -0.5 and as "Poor" otherwise. If there are more than six imputed values for a dose-response curve, the pIC<sub>50</sub> values are classified as "Poor." The workflow outputs  $R^2$  values for each fit, which should be used only with caution as this metric is inappropriate for nonlinear fits (37). It is only included to more closely match output by other statistical software. LFQ intensity histogram plots are generated highlighting each protein to visualize the relative abundance. MS/MS counts and unique peptide counts, averaged per replicate, are plotted per concentration of inhibitor to show available MS evidence for each plotted intensity. Finally, a phylogenetic tree is generated based on the seminal article of Manning et al. (1) and data visualization tools developed in the Phanstiel laboratory (38). All plots are exported as scaled vector graphic files and together with the curve fits written to a Microsoft Excel file.

The data processing workflow together with installation instructions and template sample lists are provided on GitHub: https://github.com/ APAJanssen/KNIME\_MaxQuant\_processing.

Cell Treatment for Chemical Proteomics Using a Probe Cocktail

One-third of the cells, specifically  $0.5 \times 10^6$  HEK293T cells and  $4 \times 10^6$  MV4-11 cells, were treated with XO44, ALX005, or ALX011 following the standard CellEKT workflow to assess the selectivity profile of dasatinib. At lysate level, the conditions were combined such that one-third of the lysate was treated with each probe per condition.

#### Nano-LC-MS Settings for Probe Cocktail Samples

Peptide samples were analyzed using a nanoElute 2 LC system (Bruker) coupled to a timsTOF HT mass spectrometer (Bruker). The sample (5 µl) was loaded on a trap column (PepMap C18, 5 mm  $\times$  0.3 mm, 5  $\mu$ m, 100 Å; Thermo Scientific) followed by elution

and separation on the analytical column (PepSep C18, 25 cm  $\times$  75  $\mu$ m, 1.5 μm, 100 Å; Bruker). A gradient of 2 to 25% solvent B (0.1% FA in ACN) in 35 min, 25 to 32% B in 5 min, 32 to 95% in 5 min, and 95% B for 10 min at a flow rate of 300 nl/min (all % values are v/v, water, TFA and ACN solvents were purchased from Biosolve, LC-MS grade). ZDV Sprayer 20 µm (Bruker) installed in the nano-electrospray source (CaptiveSpray source; Bruker) was used with the following source parameters: 1600 V of capillary voltage, 3.0 l/min of dry gas, and 180 °C of dry temperature. The MS data were acquired in DDA-parallel accumulation serial fragmentation (PASEF) mode with an ion mobility window of 0.85 to 1.35 Vs/cm2 in a mass range from 100 m/z to 1700 m/z with charge states from 0 to 5+. The dual TIMS analyzer was utilized under a fixed duty cycle, incorporating a 100 ms ramp time, resulting in a total cycle time of 1.17 s. Precursors that reached a target intensity of 20,000 (intensity threshold 2500) were selected for fragmentation and dynamically excluded for 0.4 min (exclusion window: mass width 0.015 m/z; 1/K0 width 0.015 Vs/cm2). The collision energy was set to 20 eV at 0.6 Vs/cm<sup>2</sup> and 59 eV at 1.6 Vs/cm<sup>2</sup>. The 1/ K0 values in between were interpolated linearly and kept constant above or below. The quadrupole isolation width was set to 2 m/z for 700 m/z and to 3 m/z for 800 m/z. Isolation width was constant except for linear interpolation between specified points. For calibration of the TIMS elution voltage, the Agilent ESI-Low Tuning Mix was used with three selected ions (m/z, 1/K0: 622.0290, 0.9915; 922.0098, 1.1986; and 1,221.9906, 1.3934). Mass calibration is performed with sodium formate in HPC mode.

#### Data Processing

The raw TIMS data (.d folders) were directly loaded into FragPipe (version 22.0; Nesvilab, University of Michigan Medical School). The FragPipe interface was used with MSFragger (39-41) (version 4.1; Nesvilab, University of Michigan Medical School), IonQuant (version 1.10.27; Nesvilab, University of Michigan Medical School), and philosopher (version 5.1.1; Nesvilab, University of Michigan Medical School) (42). The analysis was performed with the standard LFQ-MBR workflow. Searches were performed against a UniProt database of the human proteome (UPID: UP000005640, 20,363 entries, downloaded August 14, 2020) including yeast enolase (P00924), streptavidin (P22629), and trypsin (P00761). Enzyme specificity was set to strict trypsin, and up to two missed cleavages were allowed. Cysteine carboxamidomethylation (+57.021464 Da) was treated as fixed modification and methionine oxidation (+15.994915 Da) and Nterminal acetylation (+42.010565 Da) as variable modifications. The mass tolerance for precursor was set to -20 to 20 ppm, and the fragment mass tolerance was set to 20 ppm. FDR at peptide and protein levels was set to 1%. The "combined\_protein.tsv" file was used for further analysis using our standard KNIME data analysis workflow with slight adjustments because of the different output. Instead of filtering for unique peptides, the output is filtered for unique spectra. Removal of reverse peptides and contaminants is no longer necessary. DMSO-treated negative versus positive control (probe treated) is calculated based on raw intensity values, and all proteins with a ratio ≥10 are considered probe targets.

#### Cell Lysate Processing for Phosphoproteomics

MV4-11 cells (20  $\times$  10<sup>6</sup>) were treated with either vehicle (n = 2, biological replicates) or midostaurin at concentrations of 100 and 10,000 nM (n = 2 for each concentration, biological replicates) and incubated at 37 °C for 60 min. The treatment and preparation of cell pellets were performed as detailed in the previous section "Cell treatment for chemical proteomics," with the exception that no probe was used and the probe incubation step was omitted



#### Sample Preparation for Phosphoproteomics

For phosphotyrosine (pY) enrichment, a total of 5 mg of protein per sample was used. A lysate of HCT116 (colon carcinoma cell line) was taken along as workflow control. Protein samples were reduced with 5 mM DTT for 30 min at 55 °C followed by alkylation using 10 mM IAA for 15 min at RT. Lysates were then diluted using three volumes of 20 mM Hepes to reduce the concentration of urea to 2 M. Samples were digested at RT overnight using 1:100 (m/m) sequencing grade trypsin (catalog no.: V5111).

After digestion, TFA was added to reach 0.1% concentration, tubes were cooled to 0 °C, and precipitate was pelleted by centrifugation (5000g, 5 min). The peptides in the supernatant were desalted using Oasis HLB columns (500 mg capacity; Waters), eluted in 0.1% TFA, 80% ACN, and lyophilized. Lyophilized phosphopeptides were dissolved in IAP (ImmunoAffinity Purification) buffer (20 mM Tris-HCl [pH 7.2], 10 mM sodium phosphate, and 50 mM NaCl) and incubated with PTMScan pY antibody-conjugated beads (p-Tyr-1000; Cell Signaling Technology) at a ratio of 4 μl slurry per mg protein at 4 °C for 2 h as previously described (43). Then, beads were pelleted by centrifugation (2000g, 30 s), supernatant was removed, and beads were washed twice with cold IAP buffer and thrice with Milli-Q water. Phosphopeptides were eluted from the beads using two 50  $\mu$ l volumes of 0.15% TFA and directly loaded on Evotips (Evosep). Peptides were concentrated in a vacuum centrifuge at 45 °C, redissolved in 0.1% FA, and an aliquot was loaded on Evotips.

#### Nano-LC-MS Settings for Phosphoproteomics Samples

LC Analysis- Peptides were separated  $\it via$  nanoflow reversed-phase LC using standardized gradients on an Evosep One liquid chromatography system (Evosep) with 0.1% FA and 0.1% FA/99.9% ACN as the mobile phases. The 30 samples per day method was used in combination with a 15 cm  $\times$  150  $\mu m$  reverse-phase column packed with 1.5  $\mu m$  C18-beads (Bruker Daltonics) connected to a 20  $\mu m$  ID fused silica emitter (Bruker Daltonics). Peptides were introduced to a timsTOF HT (Bruker Daltonics) using a nano-electrospray ion source (Captive spray source; Bruker Daltonics) with spray voltage set to 1500 V.

MS Analysis - Peptides were analyzed on a TimsTOF HT running in DDA-PASEF mode. The ramp time was set to 100 ms, and 10 PASEF scans were acquired per topN acquisition cycle, resulting in a cycle time of 1.16 s. Precursors with a mass range from 100 m/z to  $1700 \, m/z$ , ion mobility range from 1.5 to 0.7 Vs cm<sup>2</sup>, and charge states from 0 (unassigned) to 5+ were analyzed. The intensity threshold was set to 2500 arbitrary units (a.u.) and target value to 20,000 a.u. Precursors that reached this target value or full scheduling capacity were excluded for 0.2 min. Singly charged precursors were filtered out based on their m/z-ion mobility position. Precursors with a mass below 700 Da were isolated with a quadrupole isolation width of 2 Th and precursors above 700 Da with a width of 3 Th. Collision energy was linearly decreased from 59 eV at 1.4 Vs cm<sup>-2</sup> to 20 eV at 0.6 Vs cm<sup>-2</sup>. For all experiments, the ion mobility dimension was calibrated linearly using three selected ions of the Agilent ESI LC/MS Tuning Mix  $(m/z, 1/K0: [322.0481, 0.7318 \text{ Vs cm}^{-2}], [622.0289, 0.9848 \text{ Vs cm}^{-2}],$ [922.0097, 1.1895 Vs cm<sup>-2</sup>]).

Phosphopeptide and -Site Identification and Quantification by LC-MS/MS—The DDA-PASEF files of immobilized metal affinity chromatography—enriched phosphopeptides were searched separately against the Swiss-Prot human FASTA file (downloaded March 2023, canonical and isoforms; 42,420 entries) using MaxQuant 2.3.1.0. The following changes were made to the standard settings of MaxQuant: enzyme specificity was set to trypsin, and up to two missed cleavages were allowed. Cysteine carboxamidomethylation

(+57.021464 Da) was treated as fixed modification and serine, threonine, and tyrosine phosphorylation (+79.966330 Da), methionine (+15.994915 Da), oxidation and N-terminal (+42.010565 Da) as variable modifications. The mass tolerance for precursor was set to 20 ppm in the first search and 4.5 ppm in the main search. The fragment mass tolerance was set to 20 ppm. FDR at peptide and protein levels was set to 1%. MBR was enabled. For calculation of kinase Integrative Kinase Activity scores (43), phosphopeptide MS/MS spectral counts were calculated from the Max-Quant evidence file using Rand used for substrate-centric inference of kinase activity on the basis of kinase-substrate relationships, which are either experimentally observed (PhosphoSitePlus) or algorithmpredicted using sequence motif and protein-protein network information (NetworKIN). After literature analysis, NPM1 was excluded as kinase substrate. For data representation and analysis, biological replicates were averaged.

#### CHEMICAL SYNTHESIS

#### Materials and General Methods

All reagents were purchased from chemical suppliers (Abovchem, Ambeed, BLD, Fisher Scientific, Fluorochem, Merck, and Sigma–Aldrich) and used without further purification. Solvents (Honeywell, VWR, and Biosolve) indicated with "dry" were stored on activated 3 Å (EtOH, ACN) or 4 Å (other solvents) molecular sieves (8–12 mesh; Acros Organics).

Microwave reactions were performed in a Biotage initiator + reactor. Reactions were monitored by TLC (silica gel 60, UV<sub>254</sub>; Macherey-Nagel, ref.: 818333), and compounds were visualized by UV absorption (254 nm and/or 366 nm) or spray reagent (permanganate [5 g/l KMnO<sub>4</sub>, 25 g/; K<sub>2</sub>CO<sub>3</sub>]) followed by heating. Alternatively, reactions were monitored by LC-MS, either on a Thermo Finnigan (Thermo Finnigan LCQ Advantage MAX ion-trap mass spectrometer [ESI+] coupled to a Surveyor HPLC system [Thermo Finnigan] equipped with a Nucleodur C18 Gravity column [50 × 4.6 mm, 3 μm particle size, Macherey-Nagel]) or a Thermo Fleet (Thermo LCQ Fleet ion-trap mass spectrometer [ESI+] coupled to a Vanquish UHPLC system). LC-MS eluent consisted of H<sub>2</sub>O in 0.1% TFA (aq.) and ACN in 0.1% TFA (aq.). LC-MS methods were as follows: 0.5 min cleaning with starting gradient, 8 min using specified gradient (linear), and 2 min cleaning with 90% ACN in 0.1% TFA (aq.). LC-MS data are reported as follows: instrument (Finnigan or Fleet), gradient (% ACN in 0.1% TFA [aq.]), retention time (t<sub>r</sub>), and mass (as m/z:  $[M + H]^+$ ). Purity of final compounds was determined to be ≥95% by integrating UV intensity of spectra generated by either of the LC-MS instruments.

 $^{1}\text{H},~^{13}\text{C},~\text{and}~^{19}\text{F}~\text{NMR}~\text{spectra}~\text{were}~\text{recorded}~\text{on}~\text{a}~\text{Bruker}~\text{AV300}~\text{(300}~[^{1}\text{H}]~\text{and}~75~\text{MHz}~[^{13}\text{C}],~\text{respectively)},~\text{Bruker}~\text{AV400}~\text{(400, 101, and 376 MHz, respectively)},~\text{Bruker}~\text{AV500}~\text{(500, 126, and 471 MHz, respectively)},~\text{or}~\text{Bruker}~\text{AV600}~\text{(600}~[^{1}\text{H}]~\text{and}~150~[^{13}\text{C}],~\text{respectively)}~\text{NMR}~\text{spectrometer}.~\text{NMR}~\text{samples}~\text{were}~\text{prepared}~\text{in}~\text{deuterated}~\text{chloroform}~\text{(CDCl}_3),~\text{deuterated}~\text{form}~\text{of}~\text{methanol}~\text{(MeOD)},~\text{or}~\text{DMSO-d}_6.~\text{Chemical}~\text{shifts}~\text{are}~\text{given}~\text{in}~\text{ppm}~\text{($\delta$)}~\text{relative}~\text{to}~\text{residual}~\text{protonated}$ 

solvent signals (CDCl<sub>3</sub>  $\rightarrow$   $\delta$  7.26 [<sup>1</sup>H],  $\delta$  77.16 [<sup>13</sup>C], MeOD  $\rightarrow$  $\delta$  3.31 [<sup>1</sup>H],  $\delta$  49.00 [<sup>13</sup>C], DMSO →  $\delta$  2.50 [<sup>1</sup>H],  $\delta$  39.52 [<sup>13</sup>C]). Data were processed by using MestReNova (version 14; Mestrelab Research S.L.U.) and are reported as follows: chemical shift ( $\delta$ ), multiplicity, coupling constant (J in Hz), and integration. Multiplicities are abbreviated as follows: s = singlet, br s = broad singlet, d = doublet, dd = doublet of doublets, t = triplet, dt = doublet of triplets, ddt = doublet of doublet of triplets, q = quartet, dq = doublet of quartets, and m = multiplet. For some molecules, about 1:1 rotamer and/or tautomer peaks were observed, resulting in additional peaks. For these compounds, chemical shifts were reported as ranges and multiplicity was denoted by "2x," followed by the multiplicities specified previously (i.e., 2x d = twice a doublet). The reported coupling constant corresponds to either of the multiplet peaks (of note, coupling constants were the same for both multiplet peaks).

Purification was done either by manual silica gel column chromatography (using 40-63 µm, 60 Å silica gel; Macherey-Nagel) or automated flash column chromatography on a Biotage Isolera machine (using prepacked cartridges with 40-63 μm, 60 Å silica gel [4, 12, 25, or 40 g]; Screening Devices).

HPLC purifications were performed on either an Agilent 1200 preparative HPLC system (equipped with a Gemini C18 column [250 × 10 mm, 5 μm particle size; Phenomenex] coupled to a 6130 quadrupole mass spectrometer) or a Waters Acquity UPLC system (equipped with a Gemini C18 column [150 × 21 mm, 5 μm particle size; Phenomenex] coupled to an SQ mass spectrometer). Specified gradients for HPLC purifications (ACN in 0.2% TFA [aq.]) were linear (5 ml/min for 12 min [Agilent] or 25 ml/min for 10 min [Waters]). Highresolution MS (HRMS) spectra were recorded through direct injection of a 1 µM sample either on a Thermo Scientific Q Exactive Orbitrap equipped with an electrospray ion source in positive mode coupled to an Ultimate 3000 system (source voltage = 3.5 kV, capillary temperature = 275 °C, resolution R = 240,000 at m/z 400, external lock, and mass range m/z = 150-2000). The eluent for HRMS measurements consisted of a 1:1 (v/v) mixture of ACN in 0.1% FA (aq.) using a flow of 25 ml/min.

#### **CHEMICAL SYNTHESIS**

#### General Procedure A—Benzylation of Piperazine Derivatives 4 to 5

Piperazine analog 4 or 5 (1 eq), corresponding benzyl bromide (1.1 eq), and DIPEA (4 eq) were dissolved in DMF (molarity indicated), and the reaction mixture was stirred at RT for the indicated time. The reaction mixture was combined with saturated NaHCO<sub>3</sub> (10 ml) and extracted with EtOAc (3 × 10 ml). The organic layer was washed with brine (10 ml), dried over MgSO<sub>4</sub>, filtered, and concentrated. Purification was performed as indicated.

4-((4-(4-((3-Cyclopropyl-1H-pyrazol-5-yl)amino)-7-(prop-2yn-1-yl)-7H-pyrrolo[2,3-d]pyrimidin-2-yl)piperazin-1-yl) methyl)benzenesulfonyl fluoride (ALX005)

The title compound was synthesized from 4 (77.0 mg, 212 µmol) and 4-(bromomethyl)benzenesulfonyl fluoride (59.1 mg, 234 µmol) according to general procedure A (molarity: 0.08 M; reaction time: 1 h). The residue was purified by preparative HPLC to afford the product as a TFA salt (57.0 mg, 90.0  $\mu$ mol, 43%). <sup>1</sup>H NMR (400 MHz, MeOD)  $\delta$  8.19 (d, J = 8.5 Hz, 2H), 7.93 (d, J = 8.3 Hz, 2H), 7.25 (d, J = 3.8 Hz, 1H), 6.74 (d, J = 3.7 Hz, 1H), 5.94 (s, 1H), 4.96 (d, J = 2.6 Hz, 2H),4.54 (s, 2H), 4.15 - 4.08 (m, 4H), 3.46 (t, J = 5.2 Hz, 4H), 2.89 (t, J = 2.5 Hz, 1H), 2.05 - 1.92 (m, 1H), 1.13 - 1.06 (m, 2H), 0.81 (dt,J = 6.9, 4.7 Hz, 2H) (splitting up of carbons in aromatic region observed). <sup>13</sup>C NMR (101 MHz, MeOD) δ 152.05, 151.73, 151.70, 150.77, 150.71, 149.14, 149.12, 148.93, 148.86, 139.14, 135.73, 135.48, 133.98, 130.28, 126.47, 101.40, 97.40, 92.29, 78.41, 74.96, 60.46, 52.28, 43.64, 34.40, 8.88, 7.61, 7.59. <sup>19</sup>F NMR (471 MHz, DMSO) δ 65.92. LC-MS (Fleet, 10%  $\rightarrow$  90%)  $t_{\rm R}$  = 4.77 min; m/z: 535.42 [M + H]<sup>+</sup>. HRMS calculated for  $C_{26}H_{27}FN_8O_2S + H^+$ : 535.20345, found 535.20300.

4-((4-(4-((3-Cyclobutyl-1H-pyrazol-5-yl)amino)-7-(prop-2vn-1-vl)-7H-pyrrolo[2,3-d]pyrimidin-2-vl)piperazin-1-vl) methyl)benzenesulfonyl fluoride (ALX011)

The title compound was synthesized from 5 (47.5 mg, 126 µmol) and 4-(bromomethyl)benzenesulfonyl fluoride (40.0 mg, 158 μmol) according to general procedure A (molarity: 0.08 M; reaction time: 1 h). The residue was purified by preparative HPLC to afford the product as a TFA salt (29.0 mg, 44.9 μmol, 37%). <sup>1</sup>H NMR (400 MHz, MeOD) δ 8.18 (d, J = 8.4 Hz, 2H), 7.94 (d, J = 8.2 Hz, 2H), 7.26 (d, J = 3.8 Hz, 2H)1H), 6.76 (d, J = 3.7 Hz, 1H), 6.12 (s, 1H), 4.97 (s, 2H), 4.52 (s, 2H), 4.19 - 4.02 (m, 4H), 3.63 (p, J = 8.6 Hz, 1H), 3.44 (t, J = 5.2 Hz, 4H), 2.90 (t, J = 2.5 Hz, 1H), 2.48 – 2.36 (m, 2H), 2.30 - 2.17 (m, 2H), 2.17 - 2.04 (m, 1H), 2.03 - 1.89 (m, 1H).

<sup>13</sup>C NMR (101 MHz, MeOD) δ 152.03, 151.78, 151.72, 151.58, 151.55, 149.07, 149.02, 139.50, 135.63, 135.37, 133.91, 130.25, 126.48, 101.46, 97.31, 93.36, 78.41, 74.96, 60.54, 52.31, 43.74, 34.41, 32.64, 30.01, 19.49. <sup>19</sup>F NMR (471 MHz, DMSO)  $\delta$  65.93. LC-MS (Fleet, 10%  $\rightarrow$  90%)  $t_{\rm R}$  = 5.72 min; m/z: 549.13 [M + H]<sup>+</sup>. HRMS calculated for C<sub>27</sub>H<sub>29</sub>FN<sub>8</sub>O<sub>2</sub>S + H<sup>+</sup>: 549.21910, found 549.21871.

#### 2,4-Dichloro-7-(prop-2-yn-1-yl)-7H-pyrrolo[2,3-d] pyrimidine (1)

2,4-Dichloro-7H-pyrrolo[2,3-d]pyrimidine (1.00 g, 5.32 mmol) and K<sub>2</sub>CO<sub>3</sub> (1.47 g, 10.6 mmol) were suspended in DMF (25.6 ml). 3-Bromoprop-1-yne (504 μl, 5.85 mmol) was added dropwise, and the mixture was stirred at RT for 16 h. The reaction mixture was combined with H2O (50 ml) and extracted with EtOAc (3 × 50 ml). The organic layers were combined, washed with brine (3 × 50 ml), dried over MgSO<sub>4</sub>, filtered, and concentrated to afford the product as an off-white solid (1.15 g, 5.09 mmol, 96%).  $^{1}$ H NMR (400 MHz, DMSO)  $\delta$  7.84 (d, J = 3.7 Hz, 1H), 6.75 (d, J = 3.6 Hz, 1H), 5.13 (d, J = 2.6 Hz, 2H), 3.52 (t, J = 2.5 Hz, 1H). <sup>13</sup>C NMR (101 MHz, DMSO)  $\delta$  151.32, 151.19, 150.50, 131.76, 116.13, 99.75, 77.91, 76.40, 34.20. LC-MS (Fleet,  $10 \rightarrow 90\%$ ):  $t_B = 7.42 \text{ min}$ ; m/z: 226.07 [M + H]<sup>+</sup>.

#### 2-Chloro-N-(3-cyclopropyl-1H-pyrazol-5-yl)-7-(prop-2-yn-1-yl)-7H-pyrrolo[2,3-d]pyrimidin-4-amine (2)

1 (300 mg, 1.33 mmol), 3-cyclopropyl-1H-pyrazol-5-amine (254 mg, 2.06 mmol), and DIPEA (464 µl, 2.65 mmol) were dissolved in tetrahydrofuran (2.13 ml) in a microwave vial and stirred at 120 °C for 12 h in the microwave. The reaction mixture was combined with H2O (10 ml) and extracted with DCM (3  $\times$  10 ml). The organic layers were combined, dried over MgSO<sub>4</sub>, filtered, and concentrated. The residue was purified by automated column chromatography (0.5% → 9% MeOH/DCM) to afford the product as a white solid (241 mg, 771  $\mu$ mol, 58%). <sup>1</sup>H NMR (400 MHz, DMSO)  $\delta$  12.18 (s, 1H), 10.33 (s, 1H), 7.28 (d, J = 3.6 Hz, 1H), 6.84 (br s, 1H), 6.41 (s, 1H), 4.97 (d, J = 2.6 Hz, 2H), 3.42 (t, J = 2.5 Hz, 1H), 1.98 -1.87 (m, 1H), 0.97 - 0.90 (m, 2H), 0.75 - 0.67 (m, 2H). <sup>13</sup>C

NMR (101 MHz, DMSO) δ 153.89, 152.37, 150.00, 147.40, 145.47, 124.74, 101.88, 100.22, 94.47, 78.86, 75.63, 33.37, 7.70, 6.94. LC-MS (Fleet, 10%  $\rightarrow$  90%)  $t_{\rm B}$  = 5.60 min; m/z:  $313.13 [M + H]^{+}$ 

N-(3-Cyclobutyl-1H-pyrazol-5-yl)-2-(piperazin-1-yl)-7-(prop-2-yn-1-yl)-7H-pyrrolo[2,3-d]pyrimidin-4-amine (3)

1 (650 mg, 2.88 mmol), 3-cyclobutyl-1H-pyrazol-5-amine (592 mg, 4.31 mmol), and Et<sub>3</sub>N (802 μl, 5.75 mmol) were dissolved in MeOH (10.0 ml) in a microwave vial and stirred at 60 °C for 36 h in the microwave. The reaction mixture was combined with H2O (10 ml) and extracted with DCM (3  $\times$  10 ml). The organic layers were combined, dried over MgSO<sub>4</sub>, filtered, and concentrated. The residue was purified by automated column chromatography (0.5% → 9% MeOH/ DCM) to afford the product as a white solid (162 mg, 496 μmol, 17%). <sup>1</sup>H NMR (400 MHz, DMSO)  $\delta$  12.24 (s, 1H), 10.36 (s, 1H), 7.29 (d, J = 3.6 Hz, 1H), 6.86 (br s, 1H), 6.55 (s, 1H), 4.97 (d, J = 2.6 Hz, 2H), 3.52 (p, J = 8.7 Hz, 1H), 3.42 (t, J = 2.5 Hz, 1H), 2.36 - 2.23 (m, 2H), 2.23 - 2.08 (m, 2H), 2.03 - 2.08 (m, 2H)1.78 (m, 2H).  $^{13}$ C NMR (101 MHz, DMSO)  $\delta$  153.86, 152.40, 149.99, 147.39, 146.93, 124.72, 101.90, 100.24, 94.97, 78.87, 75.63, 3f3.38, 31.26, 29.04, 18.15. LC-MS (Fleet, 10% → 90%)  $t_{\rm R} = 6.06$  min; m/z: 327.13 [M + H]<sup>+</sup>.

N-(3-Cyclopropyl-1H-pyrazol-5-yl)-2-(piperazin-1-yl)-7-(prop-2-yn-1-yl)-7H-pyrrolo[2,3-d]pyrimidin-4-amine (4)

2 (262 mg, 0.838 mmol) and piperazine (289 mg, 3.35 mmol) were dissolved in DMF (13.1 ml) in a microwave vial, and the reaction mixture was stirred in the microwave at 100 °C for 18 h. The reaction mixture was combined with EtOAc (30 ml) and washed with saturated NH<sub>4</sub>Cl (30 ml), saturated NaHCO<sub>3</sub> (30 ml), and brine (30 ml). The organic layer was dried over MgSO<sub>4</sub>, filtered, and concentrated. The residue was purified by automated column chromatography (10% → 20% MeOH/ DCM) to afford the product as yellow crystals (87.0 mg, 240 μmol, 29%). (NH of piperazine not observed), 1H NMR (400 MHz, DMSO) δ 12.00 (br s, 1H), 9.60 (s, 1H), 6.87 (d, J = 3.6 Hz, 1H), 6.66 (s, 1H), 6.32 (s, 1H), 4.83 (d, J = 2.5 Hz, 2H), 3.67 - 3.60 (m, 4H), 3.33 (t, J = 2.5 Hz, 1H), 2.79 - 2.72 (m, 4H), 1.94 - 1.83 (m, 1H), 0.98 - 0.89 (m, 2H), 0.70 - 0.62 (m, 2H). <sup>13</sup>C NMR (101 MHz, DMSO) δ 158.70, 153.16, 151.72, 147.59, 145.87, 120.46, 99.89, 96.36, 93.19, 79.66, 74.86, 45.28, 45.03, 32.34, 7.89, 7.13. LC-MS (Fleet,  $10\% \rightarrow 90\%$ )  $t_{\rm B} = 4.25 \text{ min; } m/z: 363.27 \text{ [M + H]}^+.$ 

N-(3-Cyclobutyl-1H-pyrazol-5-yl)-2-(piperazin-1-yl)-7-(prop-2-yn-1-yl)-7H-pyrrolo[2,3-d]pyrimidin-4-amine (5)

3 (162 mg, 0.496 mmol) and piperazine (171 mg, 1.78 mmol) were dissolved in DMF (5.00 ml) in a microwave vial, and the reaction mixture was stirred in the microwave at 130 °C for 18 h. The reaction mixture was combined with EtOAc (10 ml) and washed with saturated NH<sub>4</sub>Cl (10 ml), saturated NaHCO<sub>3</sub> (10 ml), and brine (10 ml). The organic layer was dried over MgSO<sub>4</sub>, filtered, and concentrated. The residue was purified by automated column chromatography (10% → 20% MeOH/ DCM) to afford the product as a dark green oil (47.5 mg, 496 μmol, 26%). (NH of piperazine and NH of pyrazole not observed). <sup>1</sup>H NMR (400 MHz, DMSO) δ 9.68 (s, 1H), 6.89 (d, J = 3.6 Hz, 1H), 6.69 (d, J = 3.7 Hz, 1H), 6.51 (s, 1H), 4.84 (d, J = 2.6 Hz, 2H, 3.78 - 3.71 (m, 4H), 3.49 (p, J = 8.5 Hz, 1H),3.34 (t, J = 2.5 Hz, 1H), 2.90 - 2.83 (m, 4H), 2.36 - 2.23 (m, 2H),2.19 - 2.05 (m, 2H), 2.02 - 1.80 (m, 2H). <sup>13</sup>C NMR (101 MHz, DMSO) δ 158.61, 153.26, 151.70, 147.71, 147.52, 120.57, 99.97, 96.52, 94.36, 79.66, 74.89, 44.78, 44.43, 32.39, 31.40, 29.10, 18.26. LC-MS (Fleet,  $10\% \rightarrow 90\%$ )  $t_B = 3.82$  min; m/z: 377.17 [M + H]+.

#### SIK2 NanoBRET TE Assay

Monoclonal HEK293 stable cell lines, expressing NanoLuc-tagged human/mouse SIK2, were established by transfection with corresponding plasmids, followed by selection with 700 μg/ml G418. The NanoBRET TE Assays were performed with commercial K4 (Promega) or in-house synthesized tracers according to the manufacturer's protocol (NanoBRET TE Intracellular Kinase Assay Kit; catalog no.: N2521; Promega).

#### SIK2 Biochemical Assay With RapidFire-MS Readout

In the presence of SIK2 and ATP, the CHK-peptide (KKKVSRSGLYRSPSMPENLNRPR with C-terminal arginine amide modification) was phosphorylated at one of the four feasible serine residues. Only one phosphorylation is observed under the assay conditions. Sixty nanoliters of each compound dilution series (12 or 24 point; dilution factor 3, generally 30 µM to 170 pM) in DMSO were transferred by

acoustic dispensing to the assay plate and 30 min preincubated (ambient temperature) after the addition of 5 µl SIK2 (0.5 nM f.c.) in assay buffer (12.5 mM Hepes [pH 7.0], 10 mM magnesium acetate, and 0.005% BSA). Substrate solution (5 μl; 10 μM f.c. CHK-peptide, 100 μM ATP f.c.) for SIK2 in assay buffer was added and incubated at ambient temperature for 45 min. FA (40 µl; 0.125%) in water was added to quench the reaction. RapidFire (RF) MS was utilized for data generation as described later. The multiple charged species (3-5 charges) for the phosphorylated and nonphosphorylated form measured by multiple reaction monitoring (API5000 or 6500+) or extracted ion current (QToF) were summed up and the ratio calculated (sum phosphorylated species/sum all species) for data evaluation. Normalization was performed by Genedata software based on the noninhibition control DMSO and the commercially available SIK inhibitor at 1 µM YKL-05-099 (CAS number: 1936529-65-5). The results of the assay are expressed in IC50s.

#### RF Setup

Samples were aspirated by vacuum for maximum 600 ms and loaded to C4-cartridge (Agilent; #G9203A) for 3000 ms at 1.5 ml/min with 0.1% FA in water. Afterward, samples were transferred to the API5000 (API6500+) or QToF mass spectrometer for 4000 ms at 1.25 ml/min 5 with 90% ACN, 9.9% water, 0.007% TFA, and 0.093% FA. The cartridge was reconditioned for additional 500 ms with 0.1% FA in water.

#### MS-Setup Sciex API5000/API6500+

All MS analyses using the following MS-setup in multiple reaction monitoring mode: electrospray positive; ion spray voltage: 4000 V; temperature: 550 °C; collision gas: 5; curtain gas: 15; Gas 1: 40; Gas 2: 42; IO EP: 10.

#### Optimization of Lysis and Copper-Catalyzed Azide-Alkyne Cycloaddition Conditions

To investigate postlysis labeling, cell pellets of THP1 cells treated with staurosporine (1  $\mu$ M, 30 min) and XO44 (1  $\mu$ M, 30 min) were lysed completely in ice-cold lysis buffer containing 50 mM Hepes (Ph 7.5), 150 mM NaCl, 1 mM MgCl<sub>2</sub>, 0.1% (w/v) Triton X-100, 1X cOmplete EDTA-free Protease Inhibitor Cocktail, and 25 U/ml benzonase (sc-202391). The lysate was aliquoted in several Eppendorf tubes and treated with 0/0.1/1% SDS as well as additional staurosporine or vehicle (0.1% DMSO). Lysates were kept on ice (0 °C) or warmed to 37 °C for 2.5 h. SDS concentrations were equalized, all lysates were allowed to reach RT, and lysates were subjected to a click reaction for 30 min with freshly prepared click mix (8.26 µl per 80 µl sample: 4.38 µl 25 mM CuSO<sub>4</sub> in MilliQ, 0.88  $\mu$ l 25 mM THPTA in DMSO, 0.2  $\mu$ l 2 mM AF647-N<sub>3</sub> [Thermo Fisher] in DMSO, and 2.6 µl 250 mM sodium ascorbate [NaAsc] in MilliQ). Samples were quenched with 4X Laemmli buffer and resolved by SDS-PAGE (10% acrylamide

gel,  $\pm 80$  min, 180 V) along with protein marker (PageRuler Plus; Thermo Fisher). In-gel fluorescence was measured in the Cy3- and Cy5-channel (Chemidoc MP; Bio-Rad), and the gels were subsequently stained with Coomassie and imaged as a loading control for normalization of fluorescence intensity.

To investigate the effect of lysis buffer components on click chemistry, cell pellets of THP1 cells treated with FP-alkyne (10 µM, 30 min) or vehicle were lysed completely in ice-cold lysis buffer A (250 mM sucrose, 20 mM Hepes [pH 7.5], 1 mM MgCl<sub>2</sub>, 1X cOmplete EDTA-free Protease Inhibitor Cocktail, and 25 U/ml benzonase [sc-202391]) or B (0.1% [w/v] Triton X-100, 20 or 50 mM Hepes [pH 7.5], 150 mM NaCl, 1 mM MgCl<sub>2</sub>, 1X cOmplete EDTA-free Protease Inhibitor Cocktail, and 25 U/ml benzonase [sc-202391]). The lysate was aliquoted in several Eppendorf tubes, and SDS was added to the indicated concentration. Two samples were incubated at 37 °C for 1 h before addition of SDS to investigate postlysis labeling. Lysates were treated with freshly prepared click mix containing either NaAsc or TCEP.HCl as reducing agent and different ratios of TCEP.HCl to CuSO<sub>4</sub>. Generally, per 40 µl of lysate was added click mix containing 2.19 µl 25 mM CuSO<sub>4</sub> in MilliQ, 1.3 μL 250 mM NaAsc in MilliQ or 1.1 μl 50 mM TCEP.HCl freshly dissolved in DPBS, 0.44 µl 25/100/200 mM THPTA in DMSO, and 0.44 µl Cy5-N<sub>3</sub>. Samples were incubated for 1 h at RT before quenching with 4X Laemmli buffer, samples were resolved on SDS-PAGE gel, and in-gel fluorescence was analyzed as described previously.

To investigate the compatibility of high SDS concentrations with trifunctional 5-carboxytetramethylrhodamine biotin-N<sub>3</sub> (TAMRA-biotin-N<sub>3</sub>) (Click Chemistry Tools), cell pellets of MV4-11 cells treated with XO44 (1 μM, 30 min) were lysed completely in ice-cold lysis buffer containing 50 mM Hepes (pH 7.5), 150 mM NaCl, 1 mM MgCl<sub>2</sub>, 0.1% (w/v) Triton X-100, 1X cOmplete EDTA-free Protease Inhibitor Cocktail, and 25 U/ml benzonase (sc-202391). The lysate was aliquoted in several Eppendorf tubes and treated with 0.2 or 1% SDS at RT for 1 h, after which freshly prepared click mix was added (3.12 μl per 40 μl lysate: 1.6 μl 25 mM CuSO<sub>4</sub> in MilliQ, 0.32 μl 25 mM THPTA in DMSO, 0.4 μl 2.5 or 10 mM TAMRA-biotin-N<sub>3</sub> in DMSO, and 0.8 μl 50 mM TCEP.HCl freshly dissolved in DPBS). Samples were incubated for 30 min or 1 h at RT before quenching with 4X Laemmli buffer, samples were resolved on SDS-PAGE gel, and in-gel fluorescence was analyzed as described previously.

#### Optimization of Pull-Down Conditions

Cell pellets of MV4-11 cells treated with XO44 (1  $\mu$ M, 30 min) were lysed completely in ice-cold lysis buffer containing 50 mM Hepes (pH 7.5), 150 mM NaCl, 1 mM MgCl<sub>2</sub>, 0.1% (w/v) Triton X-100, 1X cOmplete EDTA-free Protease Inhibitor Cocktail, and 25 U/ml benzonase (sc-202391). Protein concentration was determined using BCA assay and set to 1.5 mg/ml. Aliquots (400  $\mu$ l) of lysate containing 0.2% SDS were made, allowed to reach RT, and subjected to a click

reaction for 30 min with freshly prepared click mix (7.8 µl per 100 μl lysate: 4 μl 25 mM CuSO<sub>4</sub> in MilliQ, 0.8 μl 25 mM THPTA in DMSO, 1  $\mu$ l 10 mM TAMRA-biotin-N<sub>3</sub> in DMSO, and 2  $\mu$ l 50 mM TCEP.HCl freshly dissolved in DPBS). Proteins were precipitated by addition of Hepes-EDTA buffer (80 μl, 50 mM Hepes, 50 mM EDTA, pH 7.5), MeOH (666 μl), CHCl<sub>3</sub> (166 μl), and MilliQ (150 µl), vortexing after each addition. After spinning down (1500g, 10 min), the upper and lower layers were aspirated and the protein pellet was resuspended in MeOH (600 ul) by sonication (Qsonica Q700 Microplate Sonicator,  $2 \times 10$  s pulses, 10% amplitude). The proteins were spun down (20,000g, 5 min), and the supernatant was discarded. The proteins were dissolved in 200 µl PBS containing 0.5% SDS and 20 mM DTT by heating to 65 °C for 15 min, after which the dissolved proteins were diluted with 200 µl PBS giving 1.5 mg/ml protein and 0.25% SDS ("Input" fraction). Avidin agarose (Pierce) or high-capacity Streptavidin agarose (Pierce) were prewashed twice with PBS + 0.5% SDS and once with PBS, divided over 1.5 ml tubes in indicated amounts, spun down (3000g, 2 min), and all liquids were aspirated without losing beads by using a gel-loading tip pushed to the bottom of the tube. The XO44-treated sample was divided over 100 µl aliquots (one-fourth of a regular pull-down sample). The sample was incubated with the beads under vigorous shaking (1300 rpm) ensuring the beads were in suspension. After indicated time points, the beads were spun down (3000g, 2 min), and the supernatant was collected, denatured using Laemmli buffer, and loaded on SDS-PAGE gel ("Supernatant" fraction). The beads were washed twice with PBS + 0.5% SDS and once with PBS, spun down (3000g, 2 min), and all liquids were aspirated without losing beads by means of a gelloading tip pushed to the bottom of the tube. Proteins were eluted from the beads by boiling (5 min, 95 °C) in 2X Laemmli buffer containing 2 mM biotin (Pierce), beads were spun down (3000g, 2 min), and sample was loaded on SDS-PAGE gel ("Elution" fraction).

Determining TE by Pull-Down, Elution, and Western Blot

MV4-11 cells in log phase were spun down (300g, 5 min) and resuspended at  $1.0 \times 10^6$  cells per mL in IMDM supplemented with 0.1% delipidated BSA and 10 mM Hepes. The cells were treated with kinase inhibitor or vehicle (0.1% DMSO) for 1 h at 37 °C after which 1 or 10 µl XO44 or vehicle (0.1% DMSO) was added and the cells were incubated for another 25 min. The cells were spun down (300g, 5 min, 37 °C), resuspended in ice-cold DBPS (1 ml), transferred to 1.5 ml Eppendorf tubes, and spun down again (1000g, 5 min, 4 °C). The supernatant was aspirated, and the cells were snap-frozen and stored at -80 °C. Cell pellets were lysed completely in 400 µl ice-cold lysis buffer containing 50 mM Hepes (pH 7.5), 150 mM NaCl, 1 mM MgCl<sub>2</sub>, 0.1% (w/v) Triton X-100, 1X cOmplete EDTA-free Protease Inhibitor Cocktail, and 25 U/ml benzonase (sc-202391). Protein concentrations were equalized, and 360 µl lysate was transferred to 2 ml Eppendorf tubes containing 40 µl 10% SDS (1% final), vortexed, and left at RT. The lysates were subjected to a click reaction for 1 h with freshly prepared click mix (31.2 μl per sample: 16 μl 25 mM CuSO<sub>4</sub> in MilliQ, 3.2 μl 25 mM THPTA in DMSO, 4  $\mu$ l 10 mM biotin-N<sub>3</sub> in DMSO, and 8  $\mu$ l 50 mM TCEP.HCI freshly dissolved in DPBS). Proteins were precipitated by addition of Hepes-EDTA buffer (80 µl, 50 mM Hepes, 50 mM EDTA, pH 7.5), MeOH (666 μl), CHCl<sub>3</sub> (166 μl), and MilliQ (150 µl), vortexing after each addition. After spinning down (1500g, 10 min), the upper and lower layers were aspirated and the protein pellet was resuspended in MeOH (600 µl) by sonication (Qsonica Q700 Microplate Sonicator, 2 × 10 s pulses, 10% amplitude). The proteins were spun down (20,000g, 5 min), and the supernatant was discarded. Th proteins were redissolved in PBS containing 0.5% SDS (200  $\mu$ l) and 5 mM DTT (65 °C, 15 min, 1000 rpm shaking). The samples were allowed to reach RT and transferred to new 1.5 ml Eppendorf tubes containing 30 µl prewashed avidin agarose slurry in 200 µl PBS. Samples were incubated under shaking for 2 h (800 rpm), spun down (3000g, 2 min), and the supernatant was discarded. Samples were washed (3 × PBS + 0.5% SDS, 1x PBS), and all PBS was aspirated without losing beads by means of a gel-loading tip pushed to the bottom of the tube. Proteins were eluted from the beads by boiling (5 min, 95 °C) in 2X Laemmli buffer containing 2 mM biotin (Pierce), beads were spun down (3000g, 2 min), and sample was loaded on a 10% SDS-PAGE gel. Proteins were resolved (±80 min, 180 V) along with protein marker (PageRuler Plus; Thermo Fisher) and transferred to a 0.2 µm polyvinylidene difluoride membrane by Trans-Blot Turbo Transfer system (Bio-Rad). Membranes were washed with Trisbuffered saline (TBS) (50 mM Tris [pH 7.5], 150 mM NaCl) and blocked with 5% (w/v) milk in TBS-T (50 mM Tris [pH 7.5], 150 mM NaCl, 0.05% [w/v] Tween-20) for 1 h at RT. Membranes were incubated with primary antibody rabbit-anti-FES (85704, Cell Signaling Technologies, 1:1000 dilution, o/n, 4 °C) in 5% (w/v) BSA in TBS-T. The membranes were then washed three times with TBS-T (5 min) and incubated with secondary goat anti-rabbit-HRP (sc-2030, Santa Cruz, 1:4000 dilution in 5% [w/v] milk in TBS-T, 3 h, RT) and washed three times with TBS-T and once with TBS. Membranes were developed in Clarity Western ECL Substrate (Bio-Rad), and chemiluminescence was detected on ChemiDoc MP (Bio-Rad) in the chemiluminescence channel and colorimetric channel for the protein marker. Images were processed using Image Lab 6.0.1 (Bio-Rad).

#### Experimental Design and Statistical Rationale

Quantification of protein abundance was done using the MaxLFQ algorithm for LFQ in MaxQuant or FragPipe. Further normalization and fitting of inhibitor dose-response values in the KNIME workflow was done using SciPy using the least squares method with trf optimizer. Throughout the article, stringent filtering criteria were applied, requiring proteins to

have at least two unique peptides detected and no more than one missing LFQ value in the positive control replicates. The number of unique peptides identified for each protein is reported in the supplemental tables for all experiments. For the selectivity screening of midostaurin, ibrutinib, acalabrutinib, zanubrutinib, and dasatinib, pIC<sub>50</sub> values were determined by generating full dose-response curves across six concentrations (0.1-10,000 nM) in duplicate. Standard deviations are reported for pIC<sub>50</sub> values, whereas dose-response curves include the number of imputed values, Hill slope, R-squared value, and fit quality (details given in supplemental Tables). A fit is classified as "Good" if 0.3 ≤ Hill slope ≤3.0,  $\sigma(p|C_{50}) \le 0.5$ , and  $p|C50 \ge Max(p[inhibitor]) 0.5$ ; otherwise, it is considered "Poor." Only plC50 values from "Good" fits are used throughout the article. Further details are provided in the "Data Analysis in KNIME" section. The use of six concentrations in duplicate resulted in high robustness across cell lines and was therefore deemed optimal.

In addition, two samples (n = 2) vehicle (negative control) and four samples (n = 4) with probe only (positive control) were included to assess protein enrichment, defined as positive control/negative control ≥2-fold. The positive control was further used for normalizing inhibitor-treated samples. Using two negative control samples ensured sufficient enrichment assessment while minimizing sample requirements, whereas four positive control samples provided optimal conditions for both enrichment evaluation and normalization.

For the cell line screening and the workflow optimization, two samples (n = 2) vehicle (negative control) and three samples (n = 3) with probe only (positive control) were included to assess protein enrichment.

For the phosphoproteomics experiment, two vehicletreated samples (n = 2) and midostaurin-treated samples at 100 and 10,000 nM (n = 2 per concentration) were analyzed. This design ensures reproducibility and allows for the identification of consistent phosphorylation changes while maintaining a feasible sample size.

Additional details of replicates and data analysis for specific experiments can be found in the figure legends or in the Experimental procedures section.

#### **RESULTS**

#### Optimization of Sample Preparation

The general chemical proteomics workflow is composed of five steps (1-5) that present individual challenges, as shown in Figure 1A. To improve these steps starting from our previously published workflow (30), covalent labeling by the probe was visualized by ligation to a fluorophore azide. The separation of proteins was done using SDS-PAGE, followed by fluorescence scanning, to compare treatment conditions. The pulldown conditions were investigated by ligating probe-bound proteins to the TAMRA-biotin-azide, allowing for the tracking of labeled proteins in supernatant and pull-down bead

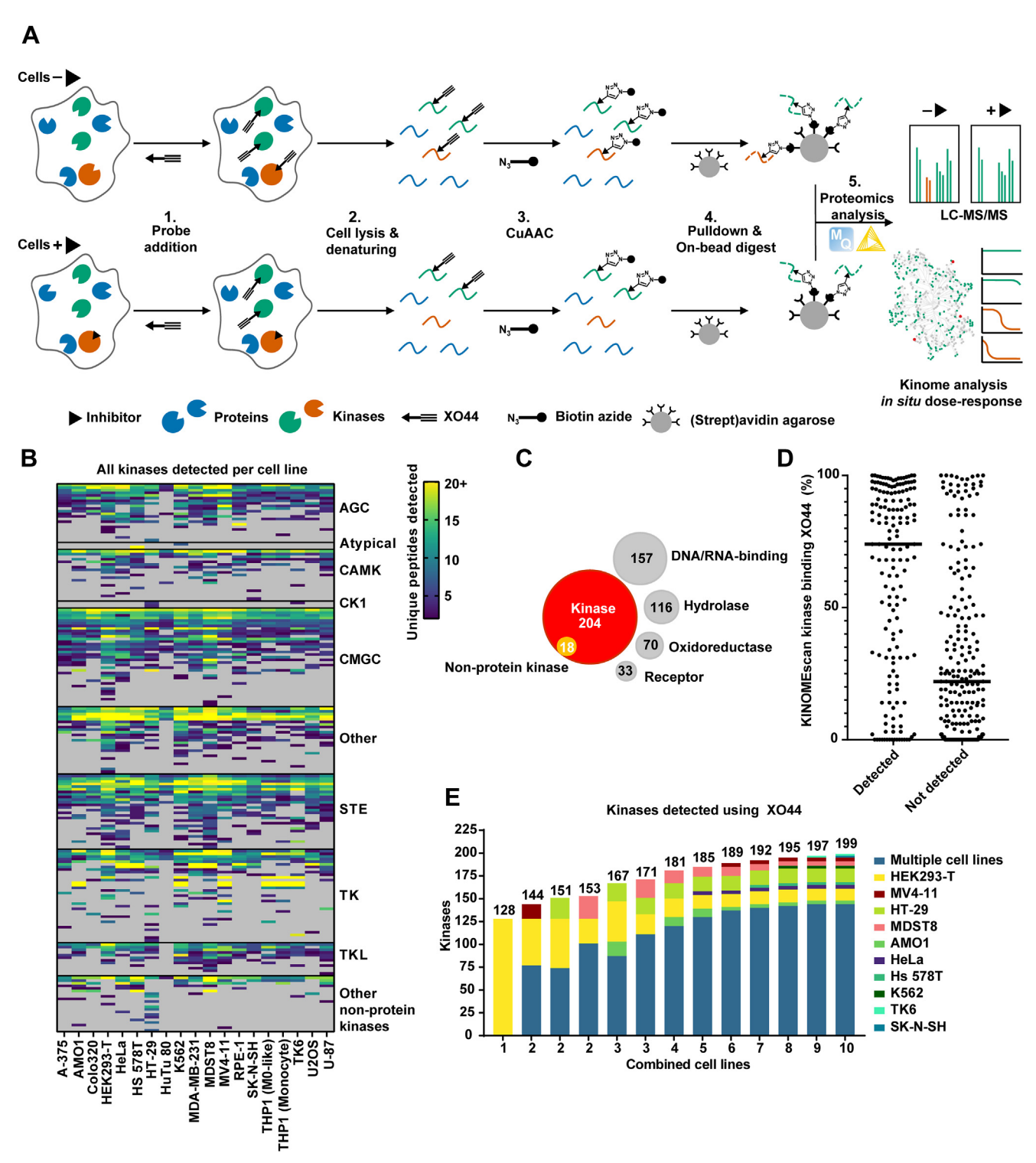


Fig. 1. Overview of chemical proteomics workflow and identification of optimal cell lines. A, graphical representation of competitive chemical proteomics workflow. B, unique peptides detected of probe-enriched kinases per cell line tested. Proteomics data are from n = 3 biological replicates of 1 µM XO44. C, molecular function analysis of all probe-enriched proteins from all tested cell lines. Main molecular functions are displayed. D, kinase binding of 1 μM XO44 as determined by KINOMEscan assay (Eurofins). Lines represent median binding values per condition. E, Kinaseblender (48) analysis of kinome coverage when combining data from different cell lines. See also Supplemental Table S1.

fractions (44). In step 1 of the workflow, the cell density was optimized by treating various concentrations of THP-1 cells with XO44 at a concentration of 1 µM to avoid the risk of probe depletion. Integration of the fluorescent signal on the SDS-PAGE gel showed that a cell density of  $1 \times 10^6$  cells/ml is ideal using 1 µM XO44 over 30 min of incubation (Supplemental Fig. S1A). In step 2, cell lysis was optimized by investigating the effect of postlysis labeling. Initial tests showed that probe labeling continued after cell lysis if the lysate was not kept on ice (Supplemental Fig. S1B). The sudden drop in ATP concentration was suspected to contribute to the postlysis labeling. Postlysis labeling was eliminated by increasing SDS concentration to 1%, and TCEP.HCl was found to be superior to NaAsc (Supplemental Fig. S2, A and B) in step 3, the copper-catalyzed azidealkyne cycloaddition ligation. The increased SDS concentration and using TCEP.HCl reduced reactive oxygen species-related band smearing (and S2C) (45). Both these adjustments were also identified as optimal in other studies (26, 28). Finally, in step 4, the pull-down of biotinylated proteins was optimized (30, 46). TAMRA-biotin-azide showed not to be compatible with higher SDS concentration of 1% and was therefore not further used for chemical proteomics experiments (Supplemental Fig. S2D). Residual protein labeling in the supernatant was examined by adjusting both the incubation time and the quantity of agarose beads (Supplemental Fig. S3, A-D). To further decrease bead usage without compromising signal detection, incorporating unmodified agarose beads helped to retain the proteins during washing. Finally, in step 5, the proteomics analysis was automated.

#### Selection of Cell Lines for Optimal Kinome Coverage

Next, we aimed to evaluate the kinome coverage of XO44 across various cell lines to identify the optimal cell lines for broad coverage and to pinpoint kinases that are sufficiently abundant to be detected only in certain cell lines. To this end, 19 cell lines of diverse origins, such as myeloid cells (K562, MV4-11, THP-1, and TK6), intestinal cells (Colo320-HSR, HT-29, MDST8, and HuTu-80), brain cells (SK-N-SH and U87), and others (A375, AMO1, HEK293T, HeLa, Hs 578T, MDA-MB-231, RPE1, and U2OS) were treated with 1 μM XO44 or vehicle and processed for chemical proteomics analysis. Notably, for each cell line, approximately 0.75 mg of protein after lysis was used as starting point for the chemical proteomics. LFQ in MaxQuant was used for protein quantification (47) with the following criteria to define a kinase as a probe target: at least two unique peptides with an LFQ intensity ratio of at least two between probe- and vehicle-treated conditions. and appearance on a reference UniProt kinase list (Keyword: Organism: 9606, Reviewed; Supplemental Table S1) (2). In total, 204 distinct probe-enriched kinases were identified across all cell lines (Fig. 1B, Supplemental Table S1). Forty-five kinases were only identified in one cell line. The majority (37%) of the probe-enriched proteins were

annotated with the keyword "kinase," whereas the largest alternatives were DNA or RNA binding, hydrolase, oxidoreductase, or receptor (Fig. 1C). To determine the binding affinity of XO44 to individual kinases, a biochemical KINOMEscan screen was performed (Fig. 1D, Supplemental Table S2). The results showed that the majority of kinases detected by the probe in the cellular screen showed also high binding affinity for XO44, with a median binding of 75%. In contrast, kinases not found in the chemical proteomics workflow generally showed lower binding, with a median binding of 21%. A Kinaseblender analysis was performed to investigate the cell lines with the highest complementarity with regard to kinome coverage (48). The cell line with the highest coverage was HEK293T (128 kinases). Combining it with an MV4-11 increased the coverage by 16 to 144 kinases (Fig. 1E), with diminishing returns observed as the number of cell lines increased further. The combination of HEK293T and MV4-11 was therefore selected for optimal coverage and ease of handling.

#### Increasing Coverage of Low Abundant Kinases

Next, we determined if the coverage of the kinome could be improved during the data analysis stage in MaxQuant. While LFQ allows for comparison across multiple samples, it has drawbacks, such as the need for consistent quantification and identification across several LC-MS runs. This can result in the inability to identify a peptide if its MS/MS spectra are of low quality or absent, leading to challenges in quantifying it. To address this issue, Cox et al. (49, 50) introduced the "match between runs" (MBR) function, which transfers peptide identifications across similar samples by matching m/z and retention time. This approach reduces peptide quantifications and enables the use of "peptide libraries"—data from samples included specifically to enhance peak identification. Although increasing the probe concentration for all samples could raise the number of labeled kinases, it would result in an underestimation of TE in competition experiments (Supplemental Fig. S4A). To facilitate peptide and kinase identification without compromising TE readouts, we created an experiment-specific "peptide library" (Fig. 2A). This method involved processing MV4-11 cells treated with a high XO44 concentration (10 μM) in the absence of an inhibitor, alongside samples with varying inhibitor concentrations and a low probe concentration (1 µM). This approach allowed for the identification of peptides in samples with a high concentration of probe, which could then be transferred to other samples, thereby increasing the efficiency of identification from 137 to 179 kinases (Fig. 2B, Supplemental Table S3) and increased peptide coverage for many others (Supplemental Fig. S4B). The kinases found only after matching were mostly low abundant, indicating poor engagement by 1 µM XO44 (Fig. 2C). The reliability of these quantifications was

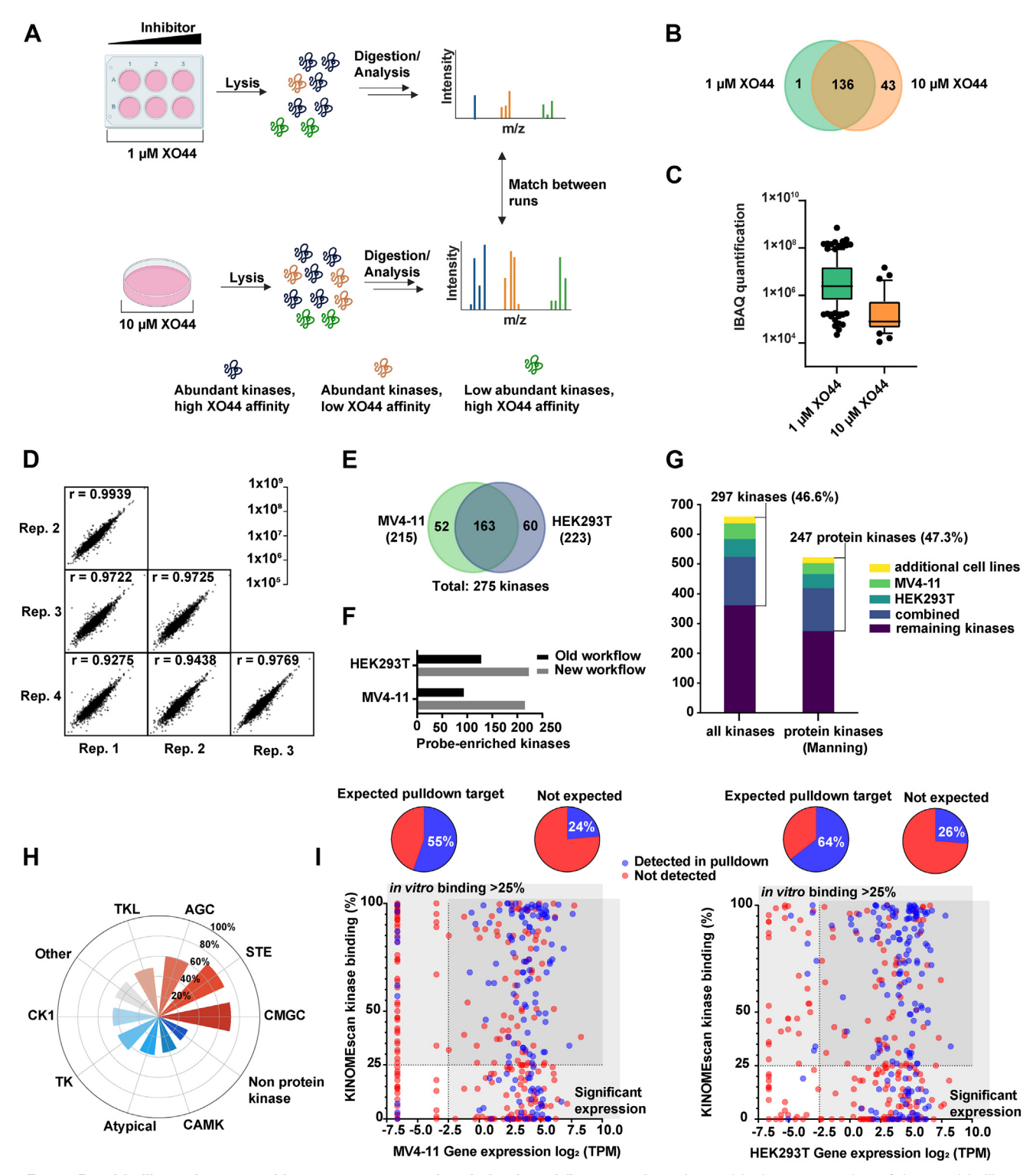


Fig. 2. Peptide library increases kinome coverage and optimized workflow overview. A, graphical representation of the peptide library. Creation of an experiment-specific peptide library, involving samples processed with high-probe concentration (10 μM) without inhibitors and samples with varying inhibitor concentrations and low-probe concentration (1 μM), enabling efficient peptide identification and enhanced kinase identification through the "MBR" function. B, probe-enriched kinases detected with high- and low-probe concentration. Increasing probe dose results in more detected kinases, indicating that at low-probe dose, these kinases are not efficiently engaged. Proteomics data are from n = 4 (1 μM XO44) and n = 2 (vehicle or 10 μM XO44) biological replicates. C, intensity-based absolute quantification (iBAQ) of probe-enriched kinases indicates kinases quantified only after matching with a peptide library have low abundance. D, comparing the intensities of matched peptides

confirmed by plotting the intensities of peptides identified by matching across replicates, which showed excellent correlation (Fig. 2D).

Finally, we optimized the loading and type of beads to reduce the streptavidin background in order to detect low abundant kinases. Using streptavidin agarose and reducing bead loading improved sequence coverage and reduced ion suppression. This refined protocol also streamlined the pulldown workflow, allowing simultaneous preparation of multiple samples (Supplemental Fig. S5, Supplemental Table S4). We tested the optimized method in MV4-11 and HEK293T cell lines. A total of 275 distinct kinases were detected, with 215 identified in MV4-11 cells and 223 in HEK293T cells (Fig. 2E, Supplemental Tables S5 and S6). The optimized workflow demonstrated an average twofold increase in kinome coverage compared with the nonoptimized workflow we previously reported (30), using the same protein input of approximately 0.75 mg (Fig. 2F). Combined with the number of kinases identified in the other cell lines of the panel screen (Supplemental Table S1), a total of 297 kinases were identified, representing nearly half of the kinome, including both protein and metabolite kinases (Fig. 2G). A similar coverage was observed when considering only the protein kinases, as defined by Manning et al. (1). XO44 exhibited varying coverage across different kinase families. The homologs of yeast sterile kinases (STE) and CMGC (named after: CDKs, mitogenactivated protein kinases, glycogen synthase kinases, and CDK-like kinases), families were the best represented, with over 70% coverage (Fig. 2H). In contrast, the nonprotein kinases, as well as the calcium/calmodulin-dependent protein kinase and atypical families, were underrepresented with less than 40% coverage. This may be due to the probe's lack of affinity for these groups' structurally unique members.

To investigate the limitations of the current kinome coverage by XO44, its binding affinities to purified kinases as measured in the KINOMEscan assay and reported mRNA expression levels (51) of HEK293T and MV4-11 were compared with the TE in the chemical proteomics experiment (Fig. 21). We could detect 55 to 64% of the kinases when we considered an in vitro binding of >25% and a gene expression level of >-2.5 log<sub>2</sub> transcript per million. This suggests that other probes with different scaffolds to XO44 may increase kinome coverage. Furthermore, kinases with low or no mRNA expression levels were generally not identified in our chemical proteomics workflow, which indicates that additional cell lines or conditions need to be screened to detect those kinases. Of

interest, 36 to 45% of the kinases targeted by XO44 in the biochemical assay were expressed in the cell lines but not detected in the chemical proteomics workflow. This suggests that the active site of those kinases was not available to the probe in the cellular context. This might be due to proteinprotein interactions, post-translational modifications, high local substrate concentrations, or the kinases were in an inactive conformation.

#### Automated Data Processing and Validation of the Workflow Using FDA-Approved Inhibitors

Next, we developed a data processing workflow using the KNIME Analytics Platform to automate the quantification of TE and selectivity profiling of kinase inhibitors. The workflow requires the MaxQuant output proteingroups.txt file, a sample list, and a list of the POIs, in this case UniProt kinases (KW-0418) (2). The workflow imputes missing data from a Gaussian distribution (36) and filters for reliable quantification, appearance on the POI list, and probe enrichment. The engagement of inhibitors is determined, and a pIC<sub>50</sub> curve is fitted through the normalized LFQ values for the POIs.

To validate our optimized chemical proteomics workflow with automated data processing, we determined the selectivity profile of the FDA-approved, reversible kinase inhibitor midostaurin, which is used for the treatment of acute myeloid leukemia and known for its broad promiscuity. Extensive selectivity data (5, 10) are available for comparison. TE was determined in a full dose-response manner across six concentrations, ranging from 0.1 nM to 10,000 nM. Each concentration was measured in biological duplicates, with the positive control and peptide library measured in biological quadruplicates and the negative control in biological duplicates. This setup enabled the generation of full doseresponse curves for each engaged and enriched kinase. Competition of kinase labeling by midostaurin was analyzed and visualized in a radar plot, grouping kinases based on their families (Fig. 3A). Midostaurin interacted with 50 kinases out of 275 enriched kinases in HEK293T and MV4-11 cells combined (Supplemental Tables S5 and S6). Midostaurin had a pIC<sub>50</sub> of  $8.15 \pm 0.16$ , on its main target FLT3 in MV4-11 cells, which is in line with its inhibitory potency in a biochemical assay. Across the kinome, pIC50 values calculated from both cell lines showed a strong correlation with the exception of Aurora Kinase A (Fig. 3B). The engagement of Aurora Kinase A by midostaurin was found to be 100-fold lower in HEK293Tcells, potentially because of differences in phosphorylation state

between replicates by Pearson's correlation indicates that matching with a peptide library results in reliable quantification results. See also Supplemental Table S3. E and F, comparing the results of pull-down experiments on HEK293T and MV4-11 cells using the old (30) and new workflow indicates a major improvement in kinome coverage with the same input material, resulting in 275 probe-enriched kinases in a single experiment. G, kinase coverage is around ~50% across all kinases (protein kinases and metabolite kinases; Keyword: KW-0418, Organism: 9606, Reviewed) (2) and Manning (1) kinases. H, illustration of kinase coverage across the different kinase families. I, comparing biochemical binding of XO44 determined by KINOMEscan assay (Supplemental Table S2) and mRNA levels of kinases from the FANTOM5 dataset (51) creates overlap of kinases, which are expected (in vitro binding of >25% and gene expression level of >-2.5 log<sub>2</sub> TPM) to be detected in a pulldown. Of those expected kinases, 55 to 64% are actually detected experimentally. See also Supplemental Tables S5 and S6. HEK293T, human embryonic kidney 293T cell line.



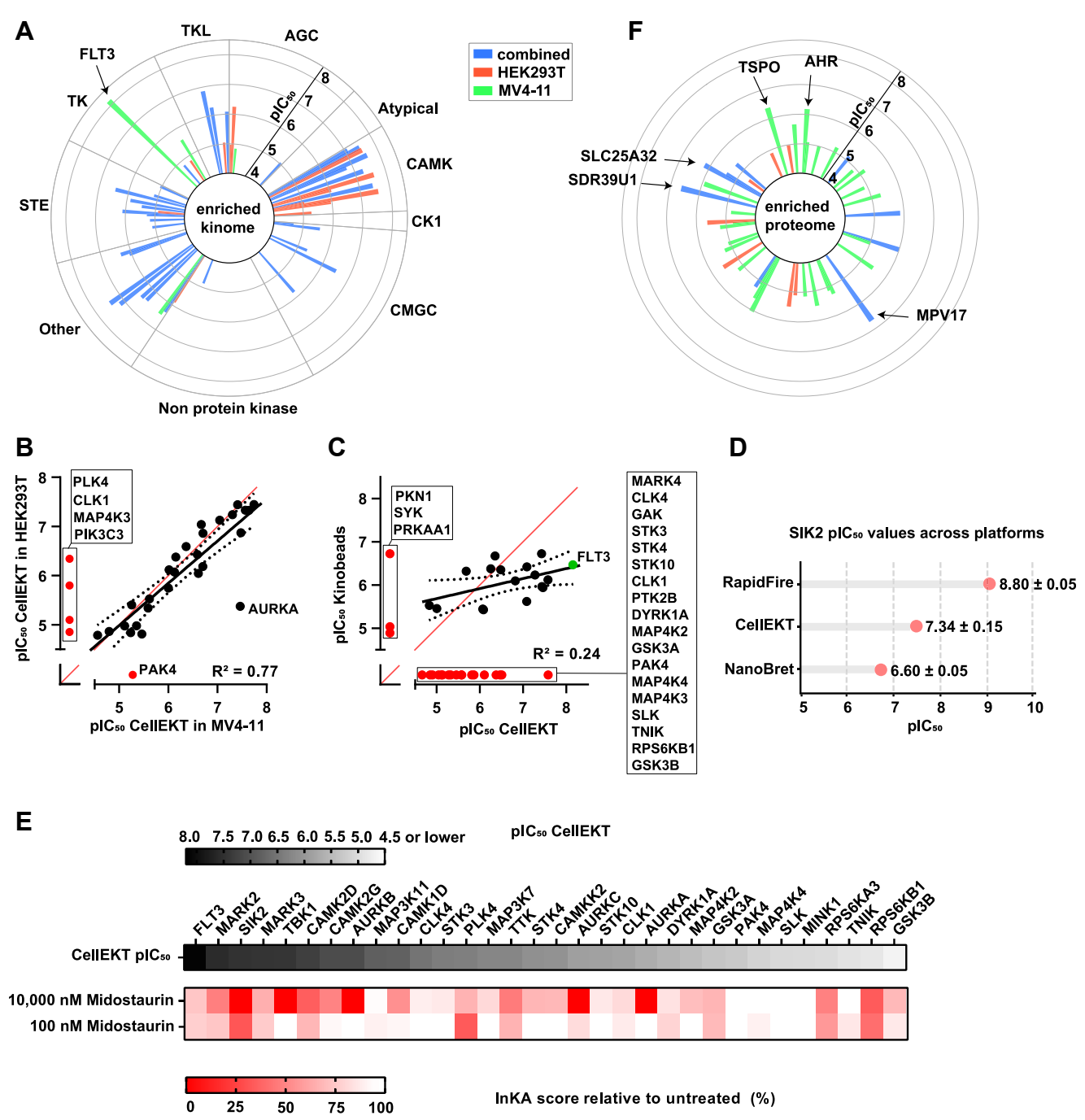


Fig. 3. Testing midostaurin in the CellEKT assay and comparison to other profiling platforms. A, radar plot depicting the kinase targets and binding affinities of midostaurin identified with a good logarithmic fit (Supplemental Tables S5 and S6). Each spike represents one target that was measured at six different concentrations from 0.1 nM to 10,000 nM, and the data are presented as mean values of n = 2 biological replicates. The length of each spike indicates the determined pIC<sub>50</sub> and the color in which cell line HEK293T (red), MV4-11 (green), or both cell lines (blue), target occupancy was determined. If target occupancy was determined in both cell lines the pIC50 values were averaged. B, correlation of kinase pIC<sub>50</sub> of midostaurin between MV4-11 and HEK293T in CellEKT assay. Kinases that were not found to be inhibited are marked in red and displayed in the corresponding box, sorted in descending order of pIC50 value. C, correlation of kinase pIC50 values of midostaurin between CellEKT (pIC<sub>50</sub> determined in MV4-11 and HEK293T combined and averaged) and Kinobeads assay (10). Kinases that were not found to be inhibited are marked in red and displayed in the corresponding box, sorted in descending order of pIC50 value. Main target is illustrated in green. The red lines depict lines of unity. D, comparison of determined pIC<sub>50</sub> values of midostaurin on SIK2 using the RapidFire, chemical proteomics, and NanoBRET platforms. E, comparison of determined pIC50 values using CellEKT, as determined in a full dose-response curve, with the effects on kinase activity and kinase substrates (INKAscore) (43) as determined by phosphoproteomics (Supplemental Table S9), conducted in n = 2 biological duplicates for each concentration. F, radar plot illustrating the targets and binding affinities of midostaurin across the enriched proteome, with the kinome excluded. CellEKT, Cellular Endogenous Kinase Targeting; HEK293T, human embryonic kidney 293T cell line.

(52). Eighteen targets of midostaurin identified using our method were not inhibited in the Kinobeads assay (10), most of which had a plC $_{50}$  value lower than 6, highlighting the sensitivity of our workflow (Fig. 3C, Supplemental Table S12). To validate a potential off-target of midostaurin, we chose SIK2 as a representative example. To this end, we compared the SIK2 engagement of midostaurin across various methods, including RF, a biochemical activity-based assay using the full-length protein, and NanoBRET (Fig. 3D). As expected, the biochemical plC $_{50}$  was significantly higher than the cellular plC $_{50}$ , but the plC $_{50}$  value in the NanoBRET was comparable to our chemical proteomics readout.

Furthermore, to correlate the TE profile with modulation of target kinase activity, we performed a phosphoproteomics experiment in MV4-11 cells using two concentrations of midostaurin (Fig. 3E). Gratifyingly, the Integrative Kinase Activity (INKA) score (43) from the phosphoproteomics data (Supplemental Table S9) correlated well with the pIC<sub>50</sub> values across the 32 targets determined by our chemical proteomics workflow. Finally, we identified also several nonkinase targets engaged by midostaurin in both cell lines (Fig. 3F, Supplemental Fig. S6A). For example, a dose-dependent inhibition of the aryl hydrocarbon receptor (AHR) (Supplemental Fig. S6B) was observed. This is in line with the previous report that midostaurin and its active metabolites are inducers of CYP1A2, an effect mediated by AHR (53). To further investigate the potential binding of XO44, we examined the crystal structure of AHR in complex with indirubin (Protein Data Bank ID: 8XSB) (54). The structure reveals that AHR contains 15 lysine residues near the binding site of indirubin, which could potentially facilitate the interaction with XO44 (Supplemental Fig. S6C).

To further validate our chemical proteomics workflow, we also profiled three FDA-approved covalent, irreversible BTK inhibitors (ibrutinib, acalabrutinib, and zanubrutinib) used for the treatment of B-lymphocyte tumors (Fig. 4, A and B) (55). All three BTK inhibitors were screened in HEK293T (Supplemental Table S7) and MV4-11 (Supplemental Table S8) cells. Ibrutinib engaged with 25 kinases, of which 10 were detected in both cell lines (Fig. 4C), with a pIC<sub>50</sub> ranging from 8.6 (BTK) to below 5 (CDK14, STK38L, LIMK1, and MAPK13). Notably, 14 kinases were identified with pIC<sub>50</sub> values below 6. Zanubrutinib engaged 16 kinases, and acalabrutinib showed the least offtargets with TEC, RIPK2, and TGFBR1. BLK, a known target of ibrutinib (56), was not enriched by XO44 and could therefore not be identified as an ibrutinib target. However, BLK enrichment was observed in AMO1 (four unique peptides) and U87 cells (15 unique peptides) (Supplemental Table S1), suggesting that BLK TE studies can be conducted in these cell lines. To validate the observed off-targets, we measured the activity of the three BTK inhibitors in a KINO-MEscan (Supplemental Table S2) and compared to the chemical proteomics profile. All engaged targets were confirmed with a general trend of reduced activity, which aligns with previous findings comparing biochemical assays to cellular activity data (25). Of note, acalabrutinib did not show any selectivity over TEC,

which is an off-target associated with an increased bleeding risk (Fig. 4B) (57). Several highly engaged ibrutinib targets, including YES1, LYN, ABL2, FYN, and SRC, identified by both CellEKT and Kinobeads, were either missed or poorly predicted by KiNative (7) (Fig. 4D, Supplemental Table S12). Comparison of ibrutinib kinase targets with Kinobeads data (10) where inhibitor treatment was performed in lysate showed good correlation (Fig. 4E). The best correlation, however, was observed for Kinobeads data (58) where inhibitor treatment was conducted in live cells, for both ibrutinib (Fig. 4F) and acalabrutinib (Supplemental Fig. S7A).

#### Additional Probes ALX005 and ALX011

Our validated chemical proteomics workflow detected 275 kinases, but as indicated previously (Fig. 2H), we missed kinases mainly from the TK, atypical, calmodulin-dependent protein kinase, and nonprotein kinase families. To address this gap, we decided to design two probes with a different scaffold from that of XO44. To this end, we converted a previously reported promiscuous kinase inhibitor (59) into two broad-spectrum probes ALX005 and ALX011 (Fig. 5A). Using a KINOMEscan (Supplemental Table S2), we confirmed that the probes had broad-spectrum kinase activity and inhibited 51 additional kinases compared with XO44 (Fig. 5B). Subsequently, we tested these probes in HEK293T and MV4-11 cells at concentrations of 1 and 10 µM (Fig. 5C, Supplemental Table S10). In total, 304 kinases were enriched across HEK293T and MV4-11 cells. Of note, ALX005 and ALX011 enriched for additional TK members such as the ephrin receptors A and B (EphB1-B3, EphA2-A4, and A7).

To exemplify the expanded kinome coverage, we determined the TE profile of the FDA-approved tyrosine kinase inhibitor dasatinib using a probe cocktail of XO44, ALX005, and ALX011 in MV4-11 cells. In this set up, we detected 29 targets of dasatinib, which were engaged with pIC<sub>50</sub> ranging from 9.1 (EPHB4) to 4.7 (MAP4K3) (Fig. 5D, Supplemental Table S11). The chemical proteomics profile correlated well ( $R^2 = 0.81$ ) with the percentage inhibition at 100 nM dasatininb measured using NanoBRET (16) (Fig. 5E). In addition, a strong correlation with Kinobeads data was observed ( $R^2 = 0.79$ ). However, five kinase targets with a pIC<sub>50</sub> >6 were not identified by the CellEKT platform, whereas DDR1 and SIK2 were identified with a poor fit (Supplemental Fig. S7B; details in Supplemental Table S12). This suggests that the inhibitors are more selective in a cellular setting compared with a cell lysate or biochemical assay. Notably, the tyrosine kinases, TNK2, EPHA2, EPHA4, and EPHB2, specifically enriched by the ALX probes, were previously not detected as off-targets by XO44. This demonstrated the complementarity of ALX005 and ALX011 to XO44.

#### Identification of the Kinase-Substrate Profiles

Our optimized chemical proteomics workflow expanded the coverage of the kinome. Consequently, we hypothesized that a broader scope of phosphosites (peptide substrates) will be covered by the kinases detected in our platform. To quantify



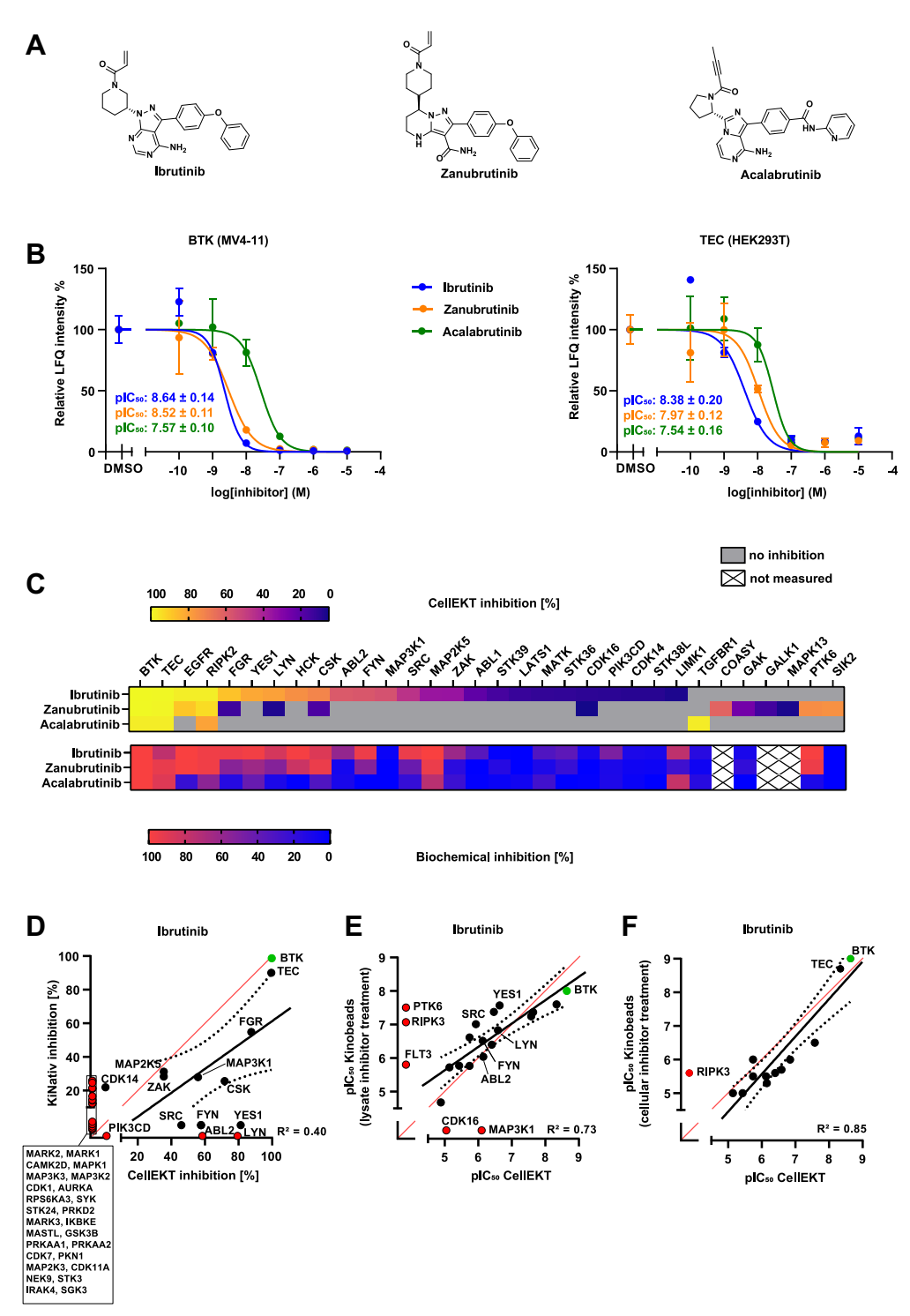


Fig 4. Selectivity profile of BTK inhibitors in the CellEKT assay and comparison to other profiling platforms. A, chemical structures of ibrutinib, zanubrutinib, and acalabrutinib. B, full dose-response curve of TEC (Supplemental Table S7) as determined in HEK293T and of BTK as determined in MV4-11 cells (Supplemental Table S8) for ibrutinib, zanubrutinib, and acalabrutinib. Target engagement is determined at six different concentrations from 0.1 nM to 10,000 nM, and data is presented as mean values ± SEM of n = 2 biological replicates. C, comparison of kinase % inhibition by CellEKT (Supplemental Tables S7 and S8) and % inhibition at 1 μM inhibitor concentration determined by KINOMEscan assay (Supplemental Table S2). For the CellEKT analysis, if a pIC<sub>50</sub> was determined in both cell lines, the values were averaged. The determined pIC<sub>50</sub> values measured by CellEKT were transformed to % inhibition by: % Inhibition = ([I]/[I] +  $10^{-pIC50}$ ) × 100 with inhibitor concentration [I] = 1 µM to match the concentration at which the KINOMEscan assay was performed. D, correlation plot comparing the KiNative dataset (7) with the percentage inhibition determined by CellEKT for ibrutinib at 1000 nM. The determined pIC50 values measured by CellEKT were transformed to % inhibition by: % Inhibition = ([I]/[I] +  $10^{-pIC50}$ ) × 100 with inhibitor concentration [I] = 1000 nM to match the concentration at which the

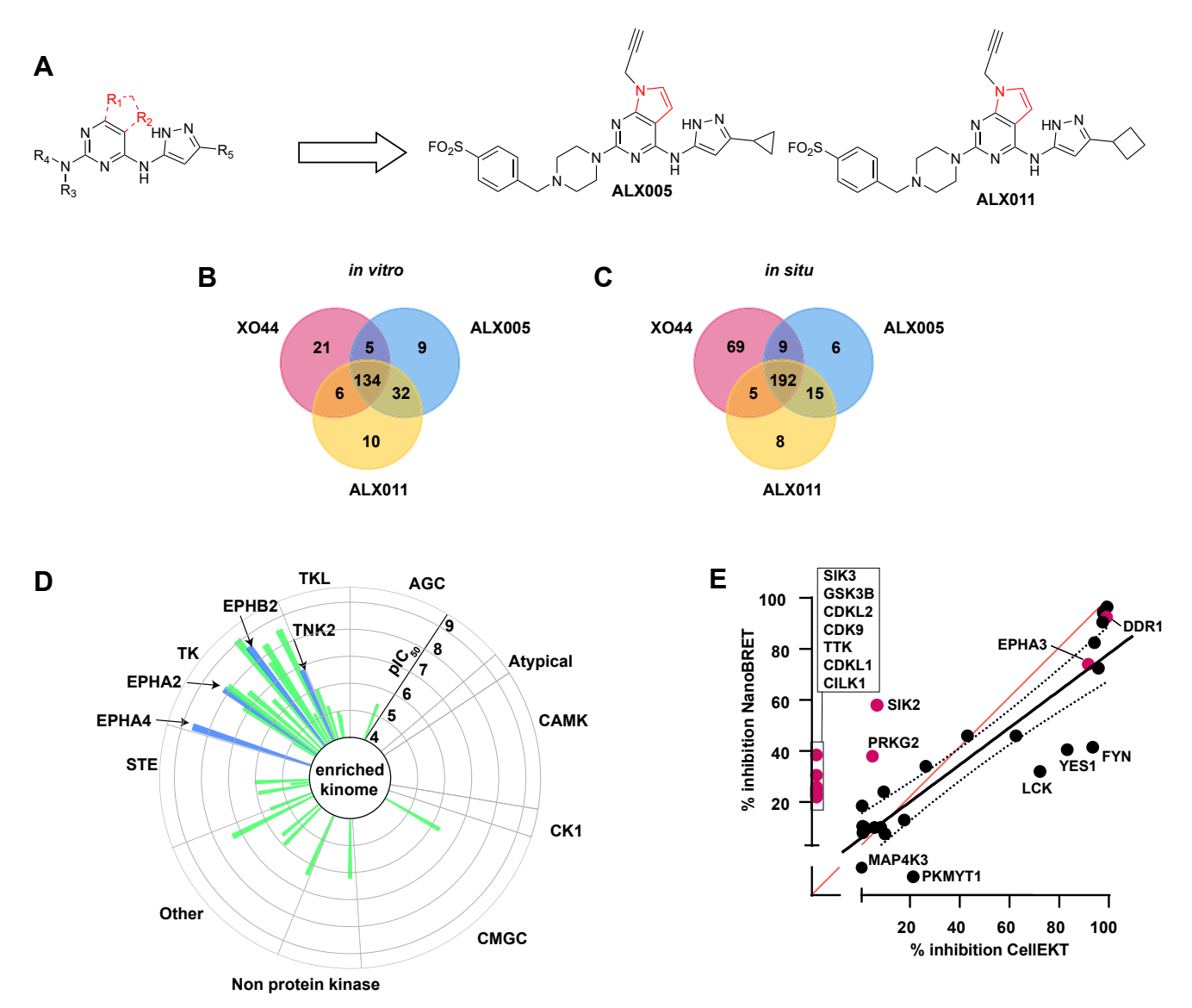


Fig 5. Profiling of ALX005/ALX011 and kinome-wide analysis using a probe cocktail to evaluate the selectivity profile of dasatinib. A. chemical structures of ALX005 and ALX011 derived from pyrrolo-pyrimidine core and XO44. B, shared and unique kinases with ≥50% inhibition at 1 µM as determined by KINOMEscan assay (Supplemental Table S2). C, shared and enriched kinases across MV4-11 and HEK293T as determined by CellEKT (Supplemental Table S10). D, radar plot depicting the kinase targets and binding affinities of dasatinib determined in MV4-11 identified with a good logarithmic fit (Supplemental Table S11). Each spike represents one target, which was measured at six different concentrations from 0.1 nM to 10,000 nM, and the data are presented as mean values of n = 2 biological replicates. The length of each spike indicates the determined pIC<sub>50</sub>. The targets identified exclusively by ALX005 and/or ALX011, as depicted in C, and demonstrating target occupancy with dasatinib are highlighted in blue. E, correlation plot comparing the percentage inhibition determined by NanoBRET (16) with the percentage inhibition determined by CellEKT. The target occupancy of dasatinib was determined at 100 nM with NanoBRET. The determined pIC<sub>50</sub> values measured by CellEKT were transformed to % inhibition by: % Inhibition =  $([1]/[1] + 10^{-pIC50}) \times 100$  with inhibitor concentration [I] = 100 nM. Kinases that were found inhibited across both platforms are illustrated in black with  $R^2 = 0.81$ . Kinases measured by NanoBRET that are not inhibited in the CellEKT assay, or have a poor logarithmic fit, are illustrated in pink. The red line depicts the line of unity. CellEKT, Cellular Endogenous Kinase Targeting.

KiNative profiling was performed. Kinases that were found not inhibited but are identified by the corresponding platform are marked in red. Main target is illustrated in green. E, correlation of kinase pIC50 values for ibrutinib between CellEKT (pIC50 determined from combined and averaged data in MV4-11 and HEK293T) and Kinobeads data, where inhibitor treatment was conducted in (E) lysate (10) and (F) live cells (58). The red lines depict lines of unity. BTK, Bruton's tyrosine kinase; CellEKT, Cellular Endogenous Kinase Targeting.

this, we compared the kinases with those for which substrate preferences have been recently studied (32, 33). Among 392 unique kinases with well-characterized substrate motifs (303 serine/threonine kinases, 93 tyrosine kinases, with four

kinases with dual specificity), 222 protein kinases are enriched by our probes (176 serine/threonine kinases and 46 tyrosine kinases). We also identified 82 enriched kinases for which substrate motifs are not yet established (Fig. 6A).

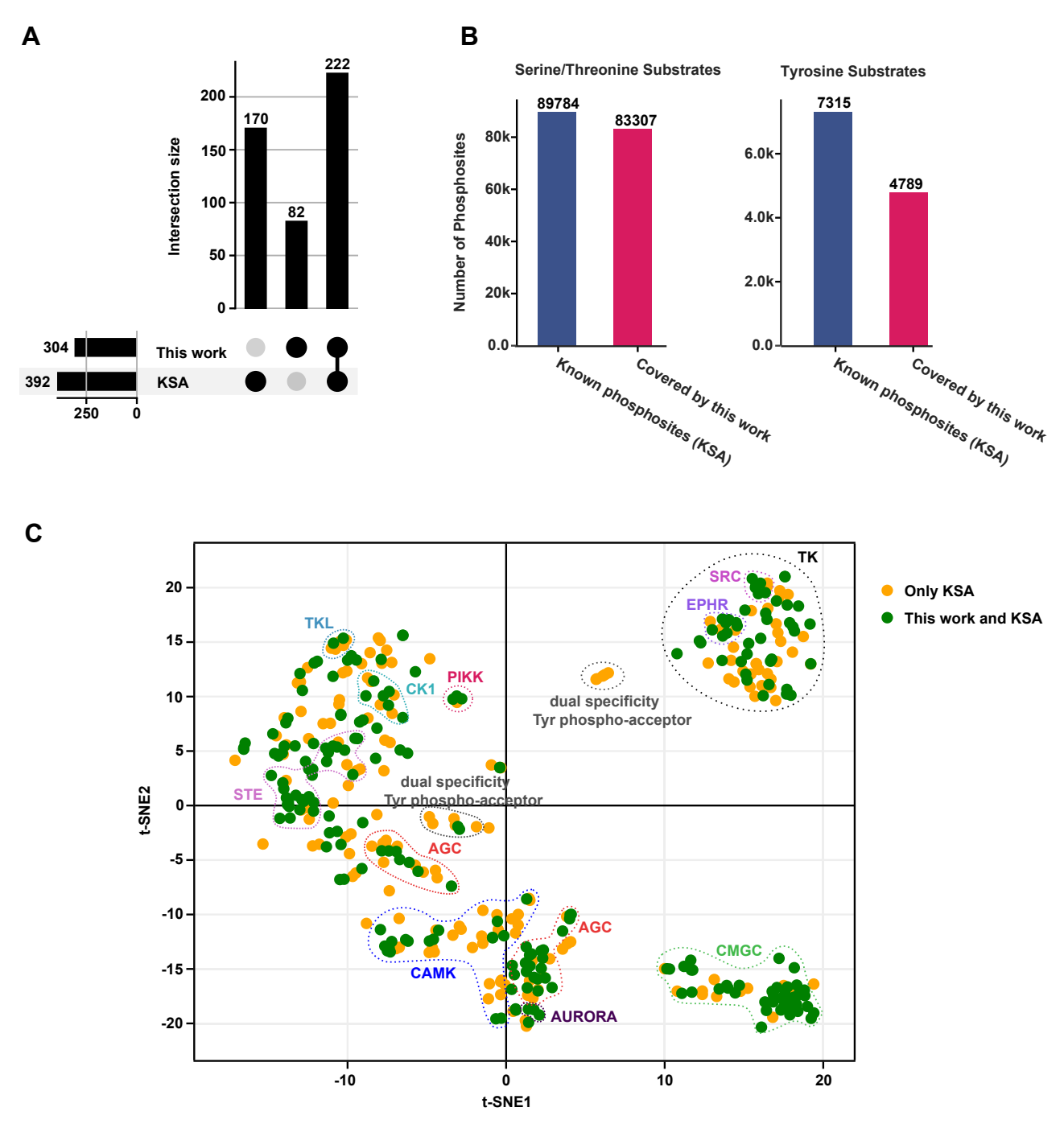


Fig 6. Expansion of the kinase-substrate coverage. A, upset plot showing kinases covered by this work compared with kinase-substrate atlas (KSA) (32, 33). The upper bar plot shows the intersection sizes, highlighting the number of kinases uniquely identified in this work, those covered by both, and those exclusive to KSA. The lower plot presents the overall counts of kinases covered by each study and their overlap. B, coverage of known serine/threonine and tyrosine phosphosites from high (60) and low-throughput (61) approaches. A substrate was considered confidently covered by a kinase if the kinase was found in the 90th percentile according to the scoring and percentile ranking from kinasesubstrate atlas (32, 33). C, t-SNE plot of kinases clustered by their amino-acid sequence preference. Each dot represents a kinase, colored orange if only covered by KSA, and green if covered by both this work and KSA. Known families of kinases are highlighted with dashed circles and labeled using reference colors from the phylogenetic tree of the human kinome. t-SNE, t-distributed stochastic neighbor embedding.

We assessed the substrate profiles of the 222 kinases with well-characterized substrate motifs, including all human phosphosites that have been demonstrated as substrates of these kinases in low-throughput and high-throughput studies (32, 33, 60, 61). Kinases engaged by our platform demonstrated a substantial coverage of the human kinase targetome (Fig. 6B), including 83,307 unique serine/threonine-containing substrates (92.7% of the known Ser/Thr kinase substrates) and 4789 tyrosine-containing substrates (65.4% of the known Tyr kinase substrates).

Moreover, we performed clustering analysis to human kinases included in the kinase–substrate atlas based on their preferred amino-acid sequences around the phosphorylation site and plot the kinases in a t-distributed stochastic neighbor embedding (t-SNE) plot by their motif similarity in Figure 6C. In the t-SNE plot, kinases with similar substrate targets are closer to each other. The 222 kinases enriched by our chemical proteomics workflow, marked in green on the t-SNE plot, show a broad coverage of the kinome (Fig. 6C).

Taken together, these observations suggests that our workflow is able to detect the majority of kinases, which are able to phosphorylate the majority of known protein substrates. It is conceivable that the kinases profiled by our platform are probably responsible for a large proportion of biological processes regulated by kinase-mediated signaling. This expansion provides valuable insights into kinase functions and their roles in various biological processes.

#### DISCUSSION

Determination of cellular TE and selectivity profiles of kinase inhibitors is crucial to understand their mode of action and to prevent adverse effects. Chemical proteomics, specifically using the XO44 probe, has advanced the study of the interaction landscape of kinase inhibitors in native biological contexts. XO44 detected 133 kinases, demonstrating its applicability for profiling kinase inhibitors (26). To advance reliable TE assessment across the endogenous kinome using chemical proteomics, a robust and standardized workflow is essential for accurate and reproducible inhibitor profiling. To address this question, we optimized the sample preparation and chemical proteomics workflow specifically for the application of XO44, building on our previously published protocol (30) for serine hydrolase profiling and the work of Taunton et al. (26, 28), to enhance detection and analysis of kinase targets. Key optimizations included refining cell density, cell lysis conditions, and ligation efficiency. Fluorescence and gel-based techniques helped track protein labeling and adjust pull-down conditions for better results. Testing across various cell lines revealed that HEK293T and MV4-11 cells

provided the best kinome coverage. Enhancements in data processing, such as implementing a peptide library using the "MBR" function, significantly increased kinase identification, particularly for low-abundance targets. Optimizing bead loading further improved detection sensitivity. Profiling using FDA-approved inhibitors validated the accuracy of the workflow, with midostaurin and three BTK inhibitors demonstrating expected TE and revealing novel off-target interactions. Furthermore, two additional probes, ALX005 and ALX011, were developed, enriching additional kinases from the tyrosine kinase subfamily and others. In total, we could detect 304 kinases (48% of kinome) with our optimized chemical proteomics workflow, which we termed CellEKT. This expanded kinome coverage allows for more comprehensive substrate profiling, providing insights into kinasemediated biological processes and potential off-target effects of kinase inhibitors. In a longer perspective, this might allow for identification of signature profiles based on more relevant quantitative inhibition and selectivity data in living cells. Thereby improving prediction and reducing major offtarget kinase liabilities such as cardiotoxicity, bone marrow toxicity, and genetic instability caused by disruption of kinase signaling.

Biochemical data may fail to predict inhibitor behavior in cells (62) and often overestimates potency, as we have confirmed for SIK2 inhibition by midostaurin (Fig. 3D). This discrepancy was also observed with lysate-based Kinobead readouts, highlighting the importance of assessing cellular inhibitor selectivity profiles (16, 25). While treating live cells with a covalent inhibitor followed by TE analysis in lysates using Kinobeads has shown strong correlation with CellEKT data for ibrutinib and acalabrutinib (Fig. 4F, Supplemental Fig. S7A), this approach is mainly restricted to covalent inhibitors that remain bound during cell lysis (58). CellEKT is able to profile cellular TE for both reversible and irreversible inhibitors similar to techniques such as NanoBRET and CETSA.

CETSA is a powerful tool for full proteome drug target screening in complex biological systems but misses targets that are not CETSA compatible and provides limited selectivity information within enzyme families such as the kinome (17). NanoBRET allows thorough evaluation of cellular kinase selectivity at thermodynamic equilibrium but is limited in flexibility for broad kinome selectivity profiling across different cell lines or in complex, native biological contexts. Conversely, CellEKT, despite its limitation in assessing TE at thermodynamic equilibrium because of the covalent nature of the probe, enables the IC<sub>50</sub> determination of an inhibitor across 304 kinases and can be applied to any cell line, primary cell, and organoid. CellEKT assesses the selectivity of a compound fully automatically across half of the kinome and other nonkinase proteins. Thus, CellEKT offers the possibility to determine cellular TE in relevant biological settings and to couple it to phenotypic or target modulations assays, such as phosphoproteomics.

Although we did not study specifically weaker affinity binders, our platform was able to capture many low-affinity interactions that correlated well with NanoBRET data. When it comes to fast  $k_{\text{off}}/\text{slow } k_{\text{on}}$  kinetic binders, CellEKT should be used with caution, and the probe incubation time or concentration needs to be optimized prior to the experiment. This may perhaps explain some of target interactions that were not identified by CellEKT but by Kinobeads.

The CellEKT platform allows to investigate the selectivity profile of a kinase inhibitor across 200+ endogenously expressed kinases in a cell line of choice. However, this still falls short of the total number of expressed kinases and relevant (off-)targets of kinase inhibitors may be missed. Moving forward, CellEKT needs to be further improved to expand its kinome coverage. In addition to the 275 enriched kinases by XO44 in HEK293T and MV4-11 cells, 100 kinases are found to be inhibited more than 20% by XO44 as determined by KINOMEscan (Supplemental Table S13). This suggests that XO44's kinase coverage is not yet fully exploited. Stimulating or synchronizing cells should lead to detectable expression levels of pulsatile expressed kinases (63). In addition, a peptide library generated using a higher probe concentration can serve as an inclusion list for DDA experiments (10, 11) and as a reference library for data-independent acquisition (64), particularly when focusing on a specific cell line and probe or probe cocktail. Future studies will explore data-independent acquisition-based approaches in combination with novel complementary probes. In addition, optimizing the workflow by incorporating magnetic beads, which have demonstrated significant benefits in enabling lower protein input while enhancing throughput (65, 66).

In conclusion, the CellEKT platform with a refined XO44 chemical proteomics workflow significantly improves the profiling of kinase inhibitor interactions within native cellular environments. CellEKT expands the kinome coverage to 48%, and its readout is validated by orthogonal biochemical assays, NanoBRET, and phosphoproteomics. A robust and versatile cellular kinase screening platform, CellEKT, can be applied to various biological contexts. Future advancements, including novel MS methods and complementary probes, are anticipated to further expand kinome coverage and enhance the role of CellEKT in supporting drug discovery and development.

#### DATA (MATERIALS AND CODE) AVAILABILITY

ALX005 and ALX011 are available upon request. The raw (phospho)proteomics datasets generated during this study are available at PRIDE (https://www.ebi.ac.uk/pride/) under the project name: "Establishing an activity-based protein profiling platform to screen in situ kinase inhibitor engagement" with

PXD035542, the accessions: PXD035544, PXD035540, PXD035549, PXD035619, PXD035550, PXD035551, PXD054026, PXD053911, and PXD055387.

The code necessary to run the automated KNIME analysis workflow along with instructions can be found at DOI: https:// doi.org/10.5281/zenodo.7656526.

Supporting information-This article contains supporting information. The following references appear in the supplemental data (10, 54, 58).

Acknowledgments—We thank the laboratory of Henk M.W. Verheul at the Radboud University Medical Center for kindly providing the HT-29 cell line, as well as laboratory of Christoph Driessen for kindly providing the AMO1 cell line. Financial support for this work was provided by F. Hoffmann-La Roche through the pRED ROADS program and the Oncode Institute. Further, support for this publication was received by Oncode Accelerator, a Dutch National Growth Fund project under grant number NGFOP2201.

Author contributions-J. R., B. G., U. G., A. C. R., and M. v. d. S. conceptualization; J. R., B. G., A. L. M., M. v. d. P., and M. S. B. methodology; J. R., B. G., A. P. A. J., A. V., and A. H. H. software; J. R., B. G., and A. A. H. validation; J. R., B. G., A. V., M. v. d. P., M. S. B., A. A. H., and B. W. formal analysis; J. R. M. v. d. S. investigation; J. R. and A. P. A. J. resources; J. R., B. G., A. P. A. J., A. V., B. I. F., A. A. H., R. H., H. W., P. W., A. T., and P. M. G. B. data curation; J. R., B. G., A. P. A. J., A. V., J. D. Z., and M. v. d. S. writing-original draft; J. R., J. P. M., C. R. J., B. W., S. K., U. G., A. C. R., and M. v. d. S. writingreview & editing; J. R., A. P. A. J., and A. V. visualization; A. P. A. J., S. K., J. D. Z., U. G., A. C. R., and M. v. d. S. supervision; J. R., B. G., U. G., A. C. R., and M. v. d. S. project administration; M. v. d. S. funding acquisition.

Conflict of interest—A. V., R. H., H. W., P. W., A. T., B. W., S. K., J. D. Z., U. G., and A. C. R. are employees of F. Hoffmann-La Roche Ltd. J. R., B. G. and M. v. d. S. are financially supported by F. Hoffmann-La Roche. Chemical probes ALX005 and ALX011 are filed as patent with J. R. and M. v. d. S. listed as inventors.

Abbreviations—The abbreviations used are: ACN, acetonitrile; AGC, automatic gain control; AHR, aryl hydrocarbon receptor; BCA, bicinchoninic acid; BRET, bioluminescence resonance energy transfer; BSA, bovine serum albumin; BTK, Bruton's tyrosine kinase; CDK, cyclin-dependent kinase; CellEKT, Cellular Endogenous Kinase Targeting; CETSA, cellular thermal shift assay; DDA, data-dependent acquisition; DIPEA, N,N-disopropylethylamine; DMEM, Dulbecco's modified Eagle's medium; DMF, dimethylformamide; DMSO, dimethyl sulfoxide; DPBS, Dulbecco's PBS; EphA/B, ephrin receptor A/B; ESI, electrospray ionization; FA, formic acid; FCS, fetal calf serum; FDA, Food and Drug Administration; FDR, false discovery rate; HEK293, human embryonic kidney 293 cell line; HRMS, high-resolution MS; IAA, iodoacetamide; IMDM, Iscove's modified Dulbecco's medium; LFQ, label-free quantitation; MBR, match between run; MeOH, methanol; MS, mass spectrometry; NaAsc, sodium ascorbate; PASEF, parallel accumulation serial fragmentation; POI, protein of interest; RF, RapidFire; RT, room temperature; TAMRA, trifunctional 5carboxytetramethylrhodamine; TBS-T, Tris-buffered saline with Tween-20; TCEP.HCl, Tris(2-carboxyethyl)phosphine hydrochloride; TE, target engagement; THPTA, Tris(3hydroxypropyltriazolylmethyl)amine; t-SNE, t-distributed stochastic neighbor embedding.

Received October 10, 2024, and in revised form, March 15, 2025 Published, MCPRO Papers in Press, April 3, 2025, https://doi.org/ 10.1016/j.mcpro.2025.100961

#### **REFERENCES**

- 1. Manning, G., Whyte, D. B., Martinez, R., Hunter, T., and Sudarsanam, S. (2002) The protein kinase complement of the human genome. Science 298, 1912-1934
- 2. Consortium, T. U., Bateman, A., Martin, M.-J., Orchard, S., Magrane, M., Ahmad, S., et al. (2022) UniProt: the Universal protein knowledgebase in 2023. Nucleic Acids Res. 51, D523-D531
- 3. Ferguson, F. M., and Gray, N. S. (2018) Kinase inhibitors: the road ahead. Nat. Rev. Drug Discov. 17, 353-377
- 4. Roskoski, R. (2024) Properties of FDA-approved small molecule protein kinase inhibitors: a 2024 update. Pharmacol. Res. 200, 107059
- 5. Davis, M. I., Hunt, J. P., Herrgard, S., Ciceri, P., Wodicka, L. M., Pallares, G., et al. (2011) Comprehensive analysis of kinase inhibitor selectivity. Nat. Biotechnol. 29. 1046-1051
- 6. Attwood, M. M., Fabbro, D., Sokolov, A. V., Knapp, S., and Schiöth, H. B. (2021) Trends in kinase drug discovery: targets, indications and inhibitor design. Nat. Rev. Drug Discov. 20, 1-23
- 7. Patricelli, M. P., Szardenings, A. K., Liyanage, M., Nomanbhoy, T. K., Wu, M., Weissig, H., et al. (2007) Functional interrogation of the kinome using nucleotide acyl phosphates. Biochemistry 46, 350-358
- 8. Patricelli, M. P., Nomanbhoy, T. K., Wu, J., Brown, H., Zhou, D., Zhang, J., et al. (2011) In situ kinase profiling reveals functionally relevant properties of native kinases. Chem. Biol. 18, 699-710
- 9. Shi, H., Zhang, C.-J., Chen, G. Y. J., and Yao, S. Q. (2012) Cell-based proteome profiling of potential dasatinib targets by use of affinity-based probes. J. Am. Chem. Soc. 134, 3001-3014
- 10. Klaeger, S., Heinzlmeir, S., Wilhelm, M., Polzer, H., Vick, B., Koenig, P.-A., et al. (2017) The target landscape of clinical kinase drugs. Science 358, eaan4368
- 11. Reinecke, M., Brear, P., Vornholz, L., Berger, B.-T., Seefried, F., Wilhelm, S., et al. (2023) Chemical proteomics reveals the target landscape of 1.000 kinase inhibitors. Nat. Chem. Biol. 20, 1-9
- 12. Bantscheff, M., Eberhard, D., Abraham, Y., Bastuck, S., Boesche, M., Hobson, S., et al. (2007) Quantitative chemical proteomics reveals mechanisms of action of clinical ABL kinase inhibitors. Nat. Biotechnol. **25** 1035–1044
- 13. Cann, M. L., McDonald, I. M., East, M. P., Johnson, G. L., and Graves, L. M. (2017) Measuring kinase activity—a global challenge. J. Cell. Biochem. **118**, 3595-3606
- 14. Wodicka, L. M., Ciceri, P., Davis, M. I., Hunt, J. P., Flovd, M., Salerno, S., et al. (2010) Activation state-dependent binding of small molecule kinase inhibitors: structural insights from biochemistry. Chem. Biol. 17, 1241-1249
- 15. Greiner, J. V., and Glonek, T. (2021) Intracellular ATP concentration and implication for cellular evolution. Biology 10, 1166
- 16. Vasta, J. D., Corona, C. R., Wilkinson, J., Zimprich, C. A., Hartnett, J. R., Ingold, M. R., et al. (2018) Quantitative, wide-spectrum kinase profiling in live cells for assessing the effect of cellular ATP on target engagement. Cell Chem. Biol. 25, 206-214.e11
- 17. Savitski, M. M., Reinhard, F. B. M., Franken, H., Werner, T., Savitski, M. F., Eberhard, D., et al. (2014) Tracking cancer drugs in living cells by thermal profiling of the proteome. Science 346, 1255784

- 18. Huber, K. V. M., Olek, K. M., Müller, A. C., Tan, C. S. H., Bennett, K. L., Colinge, J., et al. (2015) Proteome-wide drug and metabolite interaction mapping by thermal-stability profiling. Nat. Methods 12, 1055-
- 19. Perrin, J., Werner, T., Kurzawa, N., Rutkowska, A., Childs, D. D., Kalxdorf, M., et al. (2020) Identifying drug targets in tissues and whole blood with thermal-shift profiling. Nat. Biotechnol. 38, 303-308
- 20. Robers, M. B., Dart, M. L., Woodroofe, C. C., Zimprich, C. A., Kirkland, T. A., Machleidt, T., et al. (2015) Target engagement and drug residence time can be observed in living cells with BRET. Nat. Commun. 6, 10091
- 21. Stoddart, L. A., Johnstone, E. K. M., Wheal, A. J., Goulding, J., Robers, M. B., Machleidt, T., et al. (2015) Application of BRET to monitor ligand binding to GPCRs. Nat. Methods 12, 661-663.
- 22. Robers, M. B., Wilkinson, J. M., Vasta, J. D., Berger, L. M., Berger, B.-T., and Knapp, S. (2021) Single tracer-based protocol for broad-spectrum kinase profiling in live cells with NanoBRET. Star Protoc. 2, 100822
- 23. Nieman, A. N., Hoffman, K. K. D., Dominguez, E. R., Wilkinson, J., Vasta, J. D., Robers, M. B., et al. (2023) Chemogenomics, methods and protocols. Methods Mol. Biol. 2706, 97-124
- 24. Schwinn, M. K., Machleidt, T., Zimmerman, K., Eggers, C. T., Dixon, A. S., Hurst, R., et al. (2018) CRISPR-mediated tagging of endogenous proteins with a luminescent peptide. ACS Chem. Biol. 13, 467-474
- 25. Robers, M. B., Friedman-Ohana, R., Huber, K., Kilpatrick, L., Vasta, J. D., Berger, B.-T., et al. (2020) Quantifying target occupancy of small molecules within living cells. Annu. Rev. Biochem. 89, 1-25
- 26. Zhao, Q., Ouyang, X., Wan, X., Gajiwala, K. S., Kath, J. C., Jones, L. H., et al. (2017) Broad-spectrum kinase profiling in live cells with lysine-targeted sulfonyl fluoride probes. J. Am. Chem. Soc. 139, 680-685
- 27. Leung, C. O. N., Yang, Y., Leung, R. W. H., So, K. K. H., Guo, H. J., Lei, M. M. L., et al. (2023) Broad-spectrum kinome profiling identifies CDK6 upregulation as a driver of lenvatinib resistance in hepatocellular carcinoma. Nat. Commun. 14, 6699
- 28. Yang, T., Cuesta, A., Wan, X., Craven, G. B., Hirakawa, B., Khamphavong, P., et al. (2022) Reversible lysine-targeted probes reveal residence timebased kinase selectivity. Nat. Chem. Biol. 18, 1-8
- 29. Tang, G., Wang, W., Zhu, C., Huang, H., Chen, P., Wang, X., et al. (2024) Global reactivity profiling of the catalytic lysine in human kinome for covalent inhibitor development. Angew. Chem. Int. Ed. 63. e202316394
- 30. Rooden, E. J. van, Florea, B. I., Deng, H., Baggelaar, M. P., Esbroeck, A. C. M. van, Zhou, J., et al. (2018) Mapping in vivo target interaction profiles of covalent inhibitors using chemical proteomics with label-free quantification. Nat. Protoc. 13, 752-767
- 31. Esbroeck, A. C. M. van, Janssen, A. P. A., Cognetta, A. B., Ogasawara, D., Shpak, G., van der Kroeg, M., et al. (2017) Activity-based protein profiling reveals off-target proteins of the FAAH inhibitor BIA 10-2474. Science 356, 1084-1087
- 32. Johnson, J. L., Yaron, T. M., Huntsman, E. M., Kerelsky, A., Song, J., Regev, A., et al. (2023) An atlas of substrate specificities for the human serine/threonine kinome. Nature 613, 759-766
- 33. Yaron-Barir, T. M., Joughin, B. A., Huntsman, E. M., Kerelsky, A., Cizin, D. M., Cohen, B. M., et al. (2024) The intrinsic substrate specificity of the human tyrosine kinome. Nature 629, 1174-1181
- 34. [preprint] Valeanu, A., Golz, V., Avila, D. W., Tzouros, M., Siebourg-Polster, J., Badi, L., et al. (2023) (2023). Kinex infers causal kinases from phosphoproteomics data. bioRxiv. https://doi.org/10.1101/2023.11.23.568445
- 35. Rappsilber, J., Mann, M., and Ishihama, Y. (2007) Protocol for micro-purification, enrichment, pre-fractionation and storage of peptides for proteomics using StageTips, Nat. Protoc. 2, 1896-1906
- 36. Tyanova, S., Temu, T., Sinitcyn, P., Carlson, A., Hein, M. Y., Geiger, T., et al. (2016) The Perseus computational platform for comprehensive analysis of (prote)omics data. Nat. Methods 13, 731-740
- 37. Spiess, A.-N., and Neumeyer, N. (2010) An evaluation of R2 as an inadequate measure for nonlinear models in pharmacological and biochemical research: a Monte Carlo approach. BMC Pharmacol. 10, 6
- 38. Metz, K. S., Deoudes, E. M., Berginski, M. E., Jimenez-Ruiz, I., Aksoy, B. A., Hammerbacher, J., et al. (2018) Coral: clear and customizable visualization of human kinome data. Cell Syst. 7, 347-350.e1
- 39. Kong, A. T., Leprevost, F. V., Avtonomov, D. M., Mellacheruvu, D., and Nesvizhskii, A. I. (2017) MSFragger: ultrafast and comprehensive peptide identification in mass spectrometry-based proteomics. Nat. Methods 14, 513-520



- 40. Teo, G. C., Polasky, D. A., Yu, F., and Nesvizhskii, A. I. (2021) Fast deisotoping algorithm and its implementation in the MSFragger search engine. J. Proteome Res. 20, 498-505
- 41. Yu, F., Haynes, S. E., Teo, G. C., Avtonomov, D. M., Polasky, D. A., and Nesvizhskii, A. I. (2020) Fast quantitative analysis of timsTOF PASEF data with MSFragger and IonQuant. Mol. Cell. Proteom. 19, 1575-1585
- 42. Leprevost, F. da V., Haynes, S. E., Avtonomov, D. M., Chang, H.-Y., Shanmugam, A. K., Mellacheruvu, D., et al. (2020) Philosopher: a versatile toolkit for shotgun proteomics data analysis. Nat. Methods 17, 869-870
- 43. Beekhof, R., Alphen, C., Henneman, A. A., Knol, J. C., Pham, T. V., Rolfs, F., et al. (2019) INKA, an integrative data analysis pipeline for phosphoproteomic inference of active kinases. Mol. Syst. Biol. 15, e8250
- 44. Kallemeijn, W. W., Lanyon-Hogg, T., Panyain, N., Grocin, A. G., Ciepla, P., Morales-Sanfrutos, J., et al. (2021) Proteome-wide analysis of protein lipidation using chemical probes: in-gel fluorescence visualization, identification and quantification of N-myristoylation, N- and S-acylation, Ocholesterylation, S-farnesylation and S-geranylgeranylation. Nat. Protoc. **16**. 5083-5122
- 45. Thinon, E., Fernandez, J. P., Molina, H., and Hang, H. C. (2018) Selective enrichment and direct analysis of protein S-palmitoylation sites. J. Proteome Res. 17, 1907-1922
- 46. Storck, E. M., Morales-Sanfrutos, J., Serwa, R. A., Panyain, N., Lanyon-Hogg, T., Tolmachova, T., et al. (2019) Dual chemical probes enable quantitative system-wide analysis of protein prenylation and prenylation dynamics. Nat. Chem. 11, 552-561
- 47. Cox, J., and Mann, M. (2008) MaxQuant enables high peptide identification rates, individualized p.p.b.-range mass accuracies and proteome-wide protein quantification. Nat. Biotechnol. 26, 1367-1372
- 48. Médard, G., Pachl, F., Ruprecht, B., Klaeger, S., Heinzlmeir, S., Helm, D., et al. (2015) Optimized chemical proteomics assay for kinase inhibitor profiling. J. Proteome Res. 14, 1574-1586
- 49. Geiger, T., Wehner, A., Schaab, C., Cox, J., and Mann, M. (2012) Comparative proteomic analysis of eleven common cell lines reveals ubiquitous but varying expression of most proteins. Mol. Cell. Proteom. 11. M111.014050
- 50. Tyanova, S., Temu, T., and Cox, J. (2016) The MaxQuant computational platform for mass spectrometry-based shotgun proteomics. Nat. Protoc. **11**. 2301-2319
- 51. Lizio, M., Harshbarger, J., Shimoji, H., Severin, J., Kasukawa, T., Sahin, S., et al. (2015) Gateways to the FANTOM5 promoter level mammalian expression atlas. Genome Biol. 16, 22
- 52. Smith, K. P., Gifford, K. M., Waitzman, J. S., and Rice, S. E. (2015) Survey of phosphorylation near drug binding sites in the Protein Data Bank (PDB) and their effects. Proteins: Struct. Funct. Bioinform 83, 25-36

- 53. Haefliger, D., Marzolini, C., Lamoth, F., Pabst, T., Buclin, T., and Livio, F. (2023) Clinically relevant bidirectional drug-drug interaction between midostaurin and voriconazole. Br. J. Clin. Pharmacol. 89, 2304-2308
- 54. Diao, X., Shang, Q., Guo, M., Huang, Y., Zhang, M., Chen, X., et al. (2025) Structural basis for the ligand-dependent activation of heterodimeric AHR-ARNT complex. Nat. Commun. 16, 1282
- 55. Estupiñán, H. Y., Berglöf, A., Zain, R., and Smith, C. I. E. (2021) Comparative analysis of BTK inhibitors and mechanisms underlying adverse effects. Front. Cell Dev. Biol. 9, 630942
- 56. Kim, E., Hurtz, C., Koehrer, S., Wang, Z., Balasubramanian, S., Chang, B. Y., et al. (2017) Ibrutinib inhibits pre-BCR+ B-cell acute lymphoblastic leukemia progression by targeting BTK and BLK. Blood 129, 1155-1165
- 57. Levade, M., David, E., Garcia, C., Laurent, P.-A., Cadot, S., Michallet, A.-S., et al. (2014) Ibrutinib treatment affects collagen and von Willebrand factor-dependent platelet functions. Blood 124, 3991-3995
- 58. Dittus, L., Werner, T., Muelbaier, M., and Bantscheff, M. (2017) Differential Kinobeads profiling for target identification of irreversible kinase inhibitors. ACS Chem. Biol. 12, 2515-2521
- 59. Grimm, S. H. (2019) Discovery of FLT3 Inhibitors for the Treatment of Acute Myeloid Leukemia. Doctoral dissertation. Leiden University
- 60. Ochoa, D., Jarnuczak, A. F., Viéitez, C., Gehre, M., Soucheray, M., Mateus, A., et al. (2020) The functional landscape of the human phosphoproteome. Nat. Biotechnol. 38, 365-373
- 61. Hornbeck, P. V., Kornhauser, J. M., Latham, V., Murray, B., Nandhikonda, V., Nord, A., et al. (2019) 15 years of PhosphoSitePlus®: integrating posttranslationally modified sites, disease variants and isoforms. Nucleic Acids Res. 47, D433-D441
- 62. Kooijman, J. J., Riel, W. E. van, Dylus, J., Prinsen, M. B. W., Grobben, Y., Bitter, T. J. J. de, et al. (2022) Comparative kinase and cancer cell panel profiling of kinase inhibitors approved for clinical use from 2018 to 2020. Front. Oncol. 12, 953013
- 63. Malumbres, M. (2011) Physiological relevance of cell cycle kinases. Physiol. Rev. 91. 973-1007
- 64. Fröhlich, K., Brombacher, E., Fahrner, M., Vogele, D., Kook, L., Pinter, N., et al. (2022) Benchmarking of analysis strategies for data-independent acquisition proteomics using a large-scale dataset comprising inter-patient heterogeneity. Nat. Commun. 13, 2622
- 65. Becker, T., Wiest, A., Telek, A., Bejko, D., Hoffmann-Röder, A., and Kielkowski, P. (2022) Transforming chemical proteomics enrichment into a high-throughput method using an SP2E workflow. JACS Au 2, 1712-
- 66. Hughes, C. S., Moggridge, S., Müller, T., Sorensen, P. H., Morin, G. B., and Krijgsveld, J. (2019) Single-pot, solid-phase-enhanced sample preparation for proteomics experiments. Nat. Protoc. 14, 68-85

